Journal Pre-proofs

Upper mantle scale enrichment of Cenozoic intraplate magmatism in Northeast Asia: He-Sr-Nd-Pb-O isotope geochemistry of the basalts around the Korean peninsula

Donghwan Kim, Hyunwoo Lee, Mi Jung Lee, Changkun Park, Andrea Luca Rizzo

PII: S1342-937X(24)00287-9
DOI: https://doi.org/10.1016/j.gr.2024.09.016
Reference: GR 3361

To appear in: *Gondwana Research*

Received Date: 19 April 2024
Revised Date: 18 September 2024
Accepted Date: 18 September 2024

Please cite this article as: D. Kim, H. Lee, M. Jung Lee, C. Park, A. Luca Rizzo, Upper mantle scale enrichment of Cenozoic intraplate magmatism in Northeast Asia: He-Sr-Nd-Pb-O isotope geochemistry of the basalts around the Korean peninsula, *Gondwana Research* (2024), doi: https://doi.org/10.1016/j.gr.2024.09.016

Upper mantle scale enrichment of Cenozoic intraplate magmatism in Northeast Asia: He-Sr-Nd-Pb-O isotope geochemistry of the basalts around the Korean peninsula

Donghwan Kim[a], Hyunwoo Lee [a,*], Mi Jung Lee[b], Changkun Park[b], Andrea Luca Rizzo[c,d]

[a]School of Earth and Environmental Sciences, Seoul National University, Seoul 08826, Republic of Korea

[b]Division of Glacier and Earth Sciences, Korea Polar Research Institute, Incheon, 21990, Republic of Korea

[c]Department of Earth and Environmental Sciences, University of Milano-Bicocca, Piazza della Scienza 1, 20126 Milano, Italy

[d]Istituto Nazionale di Geofisica e Vulcanologia, Sezione di Milano, Via Alfonso Corti 12, 20133 Milano, Italy

*Corresponding author: Hyunwoo Lee (lhw615@snu.ac.kr)

Mailing address: School of Earth and Environmental Sciences, Seoul National University, Seoul 08826, Republic of Korea

Keywords: Helium isotopes; Radiogenic isotopes; Oxygen isotopes; Intraplate volcanism; Enriched mantle components

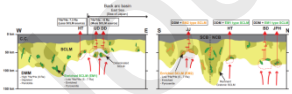

Abstract

The Earth's mantle is considered to be geochemically heterogeneous, which is reflected by the diverse composition of oceanic island basalts (OIB). The mantle enrichment resulting in this is attributed primarily to the influx of recycled crustal materials into the mantle through subduction. Additionally, the sub-continental lithospheric mantle (SCLM) complicates the elucidation of mantle heterogeneity. From this perspective, Northeast Asia, where the Pacific stagnant slab in the mantle transition zone and the SCLM distribution are presented, is the

suitable site for examining the upper mantle scale enrichment. Here we report He-Sr-Nd-Pb-O isotope values of basalts that erupted around the Korean Peninsula to illustrate the source lithology and components that led to mantle heterogeneity. Our measured helium isotope ratios ranging from 5.7 to 7.3 R_a ($^3He/^4He$ ratio of air, $R_a = 1.39 \times 10^{-6}$) are mostly within the SCLM range (6.1±0.9 R_a) but lower than the mid-ocean ridge basalt range (MORB; 8±1 R_a). The Sr-Nd-Pb isotope compositions of the basalts generally display a mixture of depleted MORB mantle (DMM), enriched mantle 1 (EM1), and enriched mantle 2 (EM2) components. In addition, the basalts have $\delta^{18}O_{olivine}$ (vs. V-SMOW) values ranging from 4.7 to 5.7 ‰ that deviate from the DMM range ($\delta^{18}O_{olivine}$ = 5.1±0.2 ‰). Our isotopic analysis results highlight the role of the pyroxenite source in the metasomatized SCLM in the genesis of basalts. The low $^3He/^4He$ range of the basalts indicates a significant role in the SCLM. Moreover, the delaminated cratonic SCLM and asthenosphere-lithosphere interaction are candidate scenarios for the low $^3He/^4He$ ratios. Therefore, we propose that mixing of DMM (high $^3He/^4He$ ratio; 7 to 9 R_a) and the metasomatized SCLM (low $^3He/^4He$ ratio; 5 to 7 R_a) allowed enrichment within the upper mantle scale for the Cenozoic intraplate magmatism in Northeast Asia.

1. Introduction

Geochemistry of radiogenic isotopes (e.g., Sr, Nd, Pb, and Hf) in oceanic island basalts (OIB) revealed the presence of mantle heterogeneity at a global scale strictly related to the Earth's mantle geodynamics (Hofmann, 2003 and references therein). Distinct geochemical reservoirs have been hypothesized mainly based on isotope compositions: i) depleted mid-ocean ridge basalt mantle (DMM; Zindler and Hart, 1986), enriched mantle type 1 (EM1), enriched mantle type 2 (EM2), and high μ ($^{238}U/^{204}Pb_{t=0}$) (HIMU; Hofmann and White, 1982) components, due to variable crustal components recycled into the mantle by subduction processes (Hawkesworth et al., 1979; Hofmann and White, 1982; Zindler and Hart, 1986). The cratonic sub-continental lithospheric mantle (SCLM) also contains recycled crustal material, characterized by enriched incompatible elements and radiogenic isotope signatures (Hawkesworth et al., 1990).

Cenozoic intraplate volcanism is widespread in Northeast Asia, including the Korean Peninsula (Chen et al., 2007). Based on radiogenic isotope compositions (e.g., Sr, Nd, Pb, and Hf) measured in basaltic rocks, various mixing patterns between DMM, EM1, and EM2 have been reported (Choi et al., 2006). Basalts from Northeast China and the Korean Peninsula (excluding Jeju Island) showed a mixture of DMM and EM1 compositions, and a hydrous plume from the mantle transition zone and/or the SCLM has been proposed for the enriched magma source (Kuritani et al., 2011; Sakuyama et al., 2014; Tian et al., 2016; Wang et al., 2011; Zhang et al., 2009). The basalts from Southeast Asia and the Jeju Island exhibit a mixing trend between DMM and EM2, and a stagnant slab, SCLM, and/or recycled sediments in the asthenosphere have been suggested for the origin of the enriched source, (Choi et al., 2006; Kim et al., 2019a; Kim et al., 2021). In addition, Cenozoic basalt samples from Northeast Asia have lower $\delta^{26}Mg$ values than that of DMM, indicating that recycled carbonate components through ancient subduction processes might have affected DMM enrichment (Kim et al., 2019a; Tian et al., 2016; Yu et al., 2018). Interestingly, all the scenarios presented are confined to the upper mantle above the mantle transition zone.

Helium isotope ratios ($^3He/^4He$) differ significantly among mantle reservoirs (e.g., Kurz et al., 1982), such as DMM (8±1 R_a; R_a is the value normalized to the $^3He/^4He$ ratio in air; Graham, 2002), SCLM (6.1±0.9 R_a; Gautheron and Moreira, 2002), and lower mantle (>9 R_a and up to ~50 R_a; Stuart et al., 2003). Thus, helium isotopes may clearly distinguish the origin of magma, the presence of contamination by crustal fluids/rocks, and the mantle source signature in relation to geodynamics. The $^3He/^4He$ values reported in previous studies of Cenozoic basalt samples in Korea suggested the possibility of involvement of SCLM in magma production (Kim et al., 2021; Lee et al., 2021). However, the evaluation of the contribution of various recycled components to produce enriched mantle components (EM1 and EM2) by helium isotope geochemistry alone has not been fully considered. In addition, recycled materials, even if not SCLM, have higher concentrations of radioactive U and Th than DMM, thus producing more radiogenic ^4He, which can decrease $^3He/^4He$ ratios in mantle/magnetic fluids (Gonnermann and Mukhopadhyay, 2009). Thus, it is necessary to incorporate the results of trace elements and radiogenic isotopes in addition to helium isotopes to comprehensively consider the contributions of recycled materials and SCLM.

For the above reasons, helium isotopes have been used to enhance understanding of local mantle properties and magma origin, along with trace element and isotope analysis in various volcanic settings (Chen et al., 2023; Dodson et al., 1998; Garapić et al., 2015; Jackson et al., 2014; Nardini et al., 2009; Oh et al., 2021). In this context, We performed a comprehensive analysis of major and trace elements, radiogenic isotopes (Sr, Nd, Pb), oxygen isotopes, and helium isotopes carried out to reveal the origins of various components recycled into the mantle beneath Northeast Asia. This study investigated the Cenozoic basalts that erupted around the Korean Peninsula, including Ulleung Island (UL), Dokdo Island (DD), Jeju Island (JJ), Baekdusan (BD), Jingpohu (JPH), and Hantangang (HT). Using the analytical results, we identify the source lithology and components responsible for the observed mantle heterogeneity to highlight its differentiation from previous studies conducted in this area of study, we perform a mantle dynamical interpretation to determine the magma origin by adding helium isotopes. In particular, we consider the metasomatized SCLM as a possible source, demonstrating that magmatism in Northeast Asia is sufficiently enriched at the upper mantle scale to have OIB-like geochemical properties.

2. Geological setting

The Korean Peninsula is located at the eastern margin of the Eurasian plate and consists of Nangrim, Gyeonggi, and Youngnam massifs of the Precambrian basement block (2.5 to 1.8 Ga; Cho et al., 2017) and bounded by Imjingang and Okcheon Fold Belts. The Imjingang Fold Belt consists of Devonian to Carboniferous metasedimentary rocks and volcanoclastic rocks over the Proterozoic basement rocks, and the Okcheon Fold Belt is made up of the metamorphosed Neoproterozoic to Paleozoic rocks as well as the weakly metamorphosed Paleozoic to early Mesozoic sedimentary rocks (Chough et al., 2000). Prior to 145 Ma in northeast North China Craton, the flat subduction of the paleo-Pacific plate occurred, accompanied by arc-related igneous activity that migrated westward (Lee et al., 2023; Liu et al., 2019; Wang et al., 2023). Extension-related magmatism began at 145 Ma and propagated to the southeastern Korean Peninsula by 80Ma, driven by the break-up of the flat subduction

and the slab roll-back (Liu et al., 2019). The cratonic lithosphere beneath North China Craton was delaminated and replaced by the juvenile SCLM due to the intensive mantle convection initiated by slab rollback and sinking (Lee et al., 2023; Wang et al., 2023). Between 80 Ma and 66 Ma, arc-related magmatism has occurred in the southeastern margin of the Korean Peninsula due to the decrease in the subduction angle (Lee et al., 2023). After 35 Ma, the Pacific plate began to subduct into the mantle transition zone, forming a big mantle wedge (Liu et al., 2019).

The Korean Peninsula became an intraplate environment after the extension of the back-arc basin from 32 to 15 Ma (Yoon et al., 2014). From the Early Oligocene (ca. 32 Ma), initial local crustal deformation started the East Sea (Sea of Japan) opening in Southeast Korea. Between approximately 28 Ma and 18 Ma, seafloor spreading led to the formation of two distinct types of back-arc basin basalts with enriched and depleted basalts in the Yamato basin, and enriched basalts in the Japan basin (Hirahara et al., 2015; Tamaki, 1995). Intensive extension of the continental crust during the early to middle Miocene (ca. 20-15 Ma) resulted in the formation of the Ulleung Basin with thick sedimentary successions with volcanic material by the south-southeastward drift of the Japanese Arc from the Korean Peninsula (Son et al., 2015; Yoon et al., 2014). At approximately 16 Ma, the back arc basin opening gradually ceased due to the onset of the subduction of the Philippine Sea Plate into the Japanese Islands (Son et al., 2015).

The JJ, UL, DD, HT, BD, and JPH volcanic activities have occurred after the termination of the back arc basin opening (Chen et al., 2007). The JJ volcanism, dominantly producing alkali and tholeiite basalts, was the submarine eruption type from 1.88 to 0.5 Ma and then began to erupt in the subaerial style from 0.5 Ma to the Holocene (Koh et al., 2013). The eruption ages of the UL and DD volcanic rocks which generated potassic alkali basalt and trachyte are known to be from 1.4 Ma to 5 Ka and 2.7 to 2.1 Ma, respectively (Lee et al., 2021, and references therein). The HT volcanic fields, formed by massive alkali basaltic lava flows erupting from Mt. Ori in North Korea can be divided into Jeongok (0.5 Ma) and Chatan (0.15 Ma) units (Ryu et al., 2011). The BD and JPH volcanic fields have erupted from the Miocene to the Holocene (Chen et al., 2007).

3. Samples and analytical methods

We analyzed 26 basalt samples from the JJ, UL, DD, HT, BD, and JPH areas (Fig. 1). All the samples are younger than 3 Ma and contain olivine and/or clinopyroxene phenocrysts. The JJ, UL, and DD rocks are the same samples as those studied by Kim et al. (2021) and Lee et al. (2021) with photographs and detailed descriptions. DB-01, DB-02, and DB-03 from JJ are massive lava units and have olivine, clinopyroxene, and plagioclase phenocrysts (Fig. S1). KB-01 and SB-01 from JJ are vesicular basalts and contain only small (< 0.5 mm) olivine phenocrysts (Fig. S1). UD-1, UD-4, DD-3, DD-1, and DD-4 are submarine volcanic rocks around the UL and DD islands. UD-2, UD-3, and DD-2 are subaerial samples. The samples from UL have euhedral to subhedral clinopyroxene, plagioclase, and oxide phenocrysts, and only UD-1 has olivine phenocrysts. All DD samples contain euhedral to subhedral olivine, clinopyroxene, plagioclase, and oxide phenocrysts. All UL and DD samples have undergone alteration, with DD-1, DD-2, and UD-1 being particularly affected. The HT basalts are from

Jeongok (0.5 Ma) and Chatan (0.15 Ma) lava units, respectively. Most of the HT samples are massive lava units with columnar or tabular joints except for CT-02 and CT-04 which are pillow basalts (Fig. S2 and Fig. S3). All the HT samples are porphyritic and intergranular and have euhedral olivine phenocrysts (Fig. S4). The BD and JPH have erupted during the Miocene, and the samples are from lava units that erupted within the last 1 Ma. The BD sample (BDS-1) is porphyritic and has mostly plagioclase phenocrysts with minor olivine phenocrysts. The JPH sample (JPH-1) is vesicular and porphyritic with olivine phenocrysts (Fig. S4).

Major and trace element compositions, and helium isotope ratios of the JJ, UL, and DD samples are from Kim et al. (2021) and Lee et al. (2021). The Sr, Nd, Pb, and O isotope ratios of the JJ, UL, and DD samples, and major and trace element compositions and He, Sr, Nd, Pb, and O isotope ratios from HT, BD, and JPH are analyzed in this study. Major element compositions of all whole-rock samples were measured by X-ray fluorescence spectrometry (Shimadzu XRF-1800) at the Cooperative Laboratory Center, Pukyong National University, Republic of Korea. For whole-rock trace element analyses of the HT basalts, we used beads made of 1g powdered rock sample and 7g $Li_2B_4O_7$ except for Pb analysis using powdered rock samples. Beads and powdered rock samples were dissolved in HF and $HClO_4$ acids. The solutions were analyzed by ICP-MS (Thermo, iCAP Q) at the Korea Polar Research Institute (KOPRI), and the mean value of three separate analyses was used as a representative value. The analytical errors in reference material (BCR-2) were within 5% of the known values. The trace elements of the other samples were analyzed by LA-ICP-MS (NWR 193 laser ablation system coupled to Agilent 7000X Inductively Coupled Plasma Mass Spectrometer) at the Korea Institute of Ocean Science and Technology (KIOST), Republic of Korea. The detailed analytical information is described in Kim et al. (2021) and Lee et al. (2021). Chemical separation and mass spectrometer analysis for Sr, Nd, and Pb isotope analysis were performed at KOPRI. The detailed laboratory procedure of this study follows Lee et al. (2015). The least altered parts were carefully chosen from crushed small pieces of 1.00 to 1.75 mm in size in a tungsten-carbide mortar. The picked samples were washed with 2N HCl in an ultrasonic bath for 10 min, to remove possible contaminants, and rinsed repeatedly with Mili-Q water. Approximately 40 to 80 mg of powdered samples, depending on the Pb concentration, were dissolved in concentrated HF and $HClO_4$ at 120°C for 3 to 4 days. Pb, Sr, and Nd were all purified from the same solution. Pb was separated from other elements using an anion exchange column with HBr medium and rinsed in 6N HCl. After Pb elution, Sr was separated by Biorad AG50W-X8 (100~200 mesh) as the ion exchange medium and collected in 2.5N HCl and 6 N HCl. Nd was separated by AG50W-X8 (200 to 500 mesh) and collected 0.2M HIBA (α-Hydroxyisobutyric acid). Collected Sr, Nd, and Pb solutions are analyzed by thermal ionization mass spectrometer (TIMS, Thermo Finnigan, TRITON) at KOPRI. Sr and Nd isotopic compositions were measured in static mode with relay matrix rotation on a single Re filament and double Re filaments, respectively. The data was corrected for mass fractionation by normalizing to $^{86}Sr/^{88}Sr = 0.1194$ and $^{146}Nd/^{144}Nd = 0.7219$ using an exponential law, and all errors were reported as 2σ of the mean. Replicate analyses of NBS 987 and Jndi-1 standards gave $^{87}Sr/^{86}Sr_{mean} = 0.710259 \pm 0.000003$ (N =100, 2σ) and $^{143}Nd/^{144}Nd_{mean} = 0.512120 \pm 0.000002$ (N = 140, 2σ). Pb isotope ratios were measured using a Pb double-spike technique with the Southampton-Brest-Lead 207-204 (SBL74) solution. Pb loaded on a single Re filament with silica gels and 0.1M H_3PO_4 and the samples were split into ~100 ng fractions for the natural run and ~10 to 15 ng fractions for the spiked mixture run, which included adding 2~3 μl of SBL74 (~10 to 15 ng Pb) to the sample Pb to obtain an optimized $^{204}Pb/^{206}Pb$ ratio of

0.5 to 2.0 in the sample-spike mixture. Replicate analyses of the NBS 981 standard gave values of (N = 100, 2σ) 36.724 ± 0.003, 15.499 ± 0.001, and 16.941 ± 0.001 for $^{208}Pb/^{204}Pb_{mean}$, $^{207}Pb/^{204}Pb_{mean}$ and $^{206}Pb/^{204}Pb_{mean}$, respectively. The total blanks averaged are 0.25 ng for Sr, 0.01 ng for Nd, and 0.03 ng for Pb, respectively. Oxygen isotope analysis of olivine phenocrysts and matrix was conducted at KOPRI using a CO_2 laser fluorination system. Olivine phenocrysts and matrix fragments of the samples, which were clean grains and fragments without any visible inclusions and impurities, were separated from the crushed and cleaned basalts by handpicking under a binocular microscope. The olivine and whole-rock samples of approximately 2 mg were vaporized using a 25W CO_2 laser with 110 mbar of BrF_5 gas. The produced oxygen gas was purified in a series of steps (Kim et al., 2019b). The oxygen isotope composition ($\delta^{18}O$ versus V-SMOW) was analyzed using a dual-inlet mass spectrometer (MAT 253 plus, Thermo Fisher Scientific). The yield of oxygen gas generation is mostly more than 85%, at least 70%. The reproducibility (2SD) of the laser fluorination system is ± 0.2 ‰ for San Carlos olivine, and ± 0.2 ‰ for MORB glass (Kim et al., 2019b).

Helium isotope ratios of the, JJ, UL, and DD basalts were previously reported by Kim et al. (2021) and Lee et al. (2021). About 1g of Olivine or clinopyroxene phenocrysts (lengths ranging from 0.25 to 1 mm) from the HT JPH, BD areas were collected by hand-picking under a binocular microscope for helium isotope analysis. The separated crystals were cleaned with distilled water and pure acetone in an ultrasonic bath before loading in the crusher system. Noble gases in fluid inclusions were released by in-vacuo single-step crushing of olivine crystals using a hydraulic press at about 200 bars to minimize the contribution of cosmogenic ^3He and radiogenic ^4He in the crystal lattice. The extracted gases were purified in an ultra-high-vacuum preparation system, which allows to removal of all the species of the gas mixture except noble gases. Argon was frozen in a charcoal trap submerged in liquid nitrogen, while He and Ne were finally separated by a cold head cooled down at 10°K. The elemental and isotopic compositions of helium (^3He and ^4He) and ^{20}Ne in olivine-hosted fluid inclusions were measured using two different split-flight-tube mass spectrometers (Helix SFT, Thermo Scientific) at the Instituto Nazionale di Geofisica e Vulcanologia (INGV) in Palermo. The $^3He/^4He$ ratios are reported in units of R/R_a, where R_a is the $^3He/^4He$ ratio of atmospheric helium and is equal to 1.39×10^{-6} (Ozima and Podosek, 2002). The $^3He/^4He$ values of HT samples are corrected for the atmospheric contamination based on the $^4He/^{20}Ne$ measured in each sample and reported as

$$R_c/R_a = ((R_M/R_a)(He/Ne)_M\text{-}(He/Ne)_A/((He/Ne)_M\text{-}(He/Ne)_A) \quad (1)$$

where M and A refer to measured and atmospheric values, respectively (e.g., Rizzo et al., 2018). The analytical uncertainty on the $^3He/^4He$ (1s) was < 1%. Details of the preparation, analysis process, and adopted standards of the samples are reported in Rizzo et al. (2018), Rizzo et al. (2022), and references therein.

4. Results

Major and trace element compositions of whole rock samples are listed in Table S1. The major and trace element contents of the DD, UL, and JJ samples were taken from Kim et al.

(2021) and Lee et al. (2021). The loss of ignition (LOI, weight %) of the samples are HT: -0.33 to 0.74, JPH: -0.3, BD: -0.5, JJ: -0.4 to 0.2, DD: 0 to 5.3 UL: 0.8 to 3.4, respectively. Negative LOI values might be due to the oxidation of FeO to Fe_2O_3, which increases the weight. Some submarine samples from UL and DD show high LOI values due to alteration. According to the total alkali versus silica (TAS) diagram (Fig. 2), most of the basalt samples, except for two sub-alkaline (tholeiitic, Kim et al., 2021) JJ basalts, are categorized into the alkaline basalt type. The samples have a wide range of MgO (1.6 to 9.0 wt%) and alkali contents (Na_2O+K_2O; 3.0 to 7.2 wt%). The Mg# [100*Mg/(Mg+Fe^{2+}) assuming Fe^{2+}/Fe^{tot} = 0.9] ranges from 29.2 to 62.9. Further details on major and trace elements for the DD, UL, and JJ samples are described in Kim et al. (2021) and Lee et al. (2021). In Fig. 3a, CI chondrite-normalized rare earth element (REE) patterns display light rare earth element (LREE) enriched trends with various $(La/Yb)_N$ ratios (6.0 to 29.0). The spider diagram normalized by the primitive mantle (PM) composition shows a similar trend to the typical OIB pattern (Fig. 3b), displaying enrichment in large ion lithophile elements (LILEs), without depletion in high field strength elements (HFSE) such as Nb and Ta. Most samples have positive anomalies for Ba, Pb, and Sr, and the HT samples have a positive anomaly for K. Measured Sr-Nd-Pb isotope compositions of the samples are shown in Table S1 and Fig. S5. In the $^{87}Sr/^{86}Sr$ versus $^{143}Nd/^{144}Nd$ plot, the JJ samples have an enrichment trend toward the EM2 end-member, and other samples have a trend close to the EM1 end-member. In Figs. S5b and S5c, the Pb isotope values of all samples appear in the upper area of the Northern Hemisphere reference line (NHRL). Similarly, the JJ samples ($^{206}Pb/^{204}Pb$ = 18.87 to 19.05, $^{207}Pb/^{204}Pb$ = 15.64 to 15.70, and $^{208}Pb/^{204}Pb$ = 39.36 to 39.67) are placed close to the EM2 end-member, while the JPH sample ($^{206}Pb/^{204}Pb$ = 17.58, $^{207}Pb/^{204}Pb$ = 15.50, and $^{208}Pb/^{204}Pb$ = 37.93) are displayed close to the EM1 end-member. The $\delta^{18}O$ values of olivine phenocrysts in the basalts range from 4.7 to 5.7 ‰ (Fig. 4 and Table S1). There are no clear correlations between the oxygen isotopes and other major elements. Most of the JJ samples have lower $\delta^{18}O$ values than the N-MORB range ($\delta^{18}O_{olivine}$ = 4.9 to 5.3 ‰, $\delta^{18}O_{whole\ rock}$ = 5.4 to 5.8 ‰), and other areas have similar and slightly higher $\delta^{18}O$ values than the N-MORB range (Eiler, 2001). The concentrations of ^4He and ^{20}Ne, the $^4He/^{20}Ne$, and the $^3He/^4He$ in olivine-hosted fluid inclusions are listed in Table S2; ^4He versus $^3He/^4He$ (R_c/R_a) are also plotted in Fig 5. The ^4He and ^{20}Ne of the HT basalts vary in a narrow range of concentration, that are 2 x 10^{-8} to 9 x 10^{-8} ccSTP/g and 2.6 x 10^{-11} to 7.1 x 10^{-11} ccSTP/g, respectively. Since the $^4He/^{20}Ne$ ratio ranges between 343 and 1,565 and this ratio in atmospheric-derived fluids is as low as 0.318 (Ozima and Podosek, 2002), corrections to the $^3He/^4He$ ratio taking into account contamination by atmospheric components are almost negligible in all samples. The $^3He/^4He$ ratios (R_c/R_a) in the HT basalts range from 6.8 to 7.3 R_a (Fig. 5), which is in between the lower limit of MORB (8±1 R_a; Graham, 2002) and the SCLM range (6.1±0.9 R_a; Gautheron and Moreira, 2002). The $^3He/^4He$ ratios (R_c/R_a) range is relatively highest in the HT basalts and is between the lower limit of MORB (8±1 Ra; Graham, 2002) and the SCLM range (6.1±0.9 R_a; Gautheron and Moreira, 2002). The $^3He/^4He$ ratios for JPH and BD are 7.2 R_a and 5.3 R_a. The $^3He/^4He$ ratios for DD, UL, and JJ reported in Kim et al. (2021) and Lee et al. (2021) are 5.7 to 5.9 R_a, 4.5 to 6.0 R_a, and 3.5 to 7.3 R_a, respectively.

5. Discussion

5.1. Pre- and post-eruption processes

The contents of MgO and major elemental oxides analyzed in our samples were plotted together with values previously reported in other studies to confirm the effect of fractional crystallization (Figs. S6 to S11). Compositional changes in the melt by fractional crystallization were investigated using Petrolog v3 software (Danyushevsky and Plechov, 2011), and the initial magma composition was based on samples with the highest MgO content in each region. It was assumed that olivine, clinopyroxene, plagioclase, and magnetite (excluding the BD and JPH regions) underwent fractional crystallization at a pressure of 7 kbar corresponding to the crust-mantle boundary depth of about 25 km beneath the Korean peninsula (Kim et al., 2015). According to the fractional crystallization model, JJ experienced fractional crystallization of olivine, clinopyroxene, and plagioclase. Fractional crystallization of olivine, clinopyroxene, and magnetite at UL and DD was followed, with most of the olivine being crystallized in particular. HT and JPH only show fractional crystallization of olivine, and BD exhibits crystallization of olivine and plagioclase.

Additionally, fractional crystallization of plagioclase and oxides can affect the trace element patterns of the samples and produce anomalies for some elements. This is attributed to that Sr, and Eu exhibit higher partition coefficients (> 1) in plagioclase depending on magma temperature and oxidation state (Sun et al., 2017), whereas HFSEs exhibit higher partition coefficients (> 1) in Ti-Fe oxides (Dygert et al., 2013). The positive anomaly observed for Ba may indicate the effect of crystallized plagioclase that remains in contact with the residual liquid, especially in UD-1 displaying Ba, Sr, and Eu anomalies (Lee et al., 2021). Nevertheless, the effect of this fractional crystallization is also considered insignificant, as most of the samples do not exhibit Eu depletion or enrichment, or HFSE (Nb and Ta) depletion.

Previous studies have shown that the basalts in Korea did not suffer from severe crustal contamination (Choi et al., 2020; Choi, 2021; Kim et al., 2019a; Lee et al., 2021; Sakuyama et al., 2014). To further verify this, our basalt samples do not exhibit negative anomalies of Nb and Ta as well as low Nb/U and Ce/Pb ratios (Fig. 6), which are characteristic of continental crustal components (Rudnick and Gao, 2003). The $^{87}Sr/^{86}Sr$ and $^{143}Nd/^{144}Nd$ values of the basalts do not show a clear correlation with the Ce/Pb ratio, indicating that there is no continental crustal component contribution with a higher $^{87}Sr/^{86}Sr$ ratios and lower $^{143}Nd/^{144}Nd$ ratios than the DMM values (Fig. 6c and d). Moreover, our samples do not show a clear tendency for the $^{3}He/^{4}He$ ratio to decrease with increasing ^{4}He, and the effect of continental crust with abundant radiogenic ^{4}He and resulting low $^{3}He/^{4}He$ ratio can be considered minimal (Fig. 5).

Several samples from UL, DD, and HT erupted underwater and might have undergone alteration due to rock-water interaction. This alteration could affect the fluid mobile elements (Ba, Rb, and K) and result in higher oxygen isotope ratios. Despite this, the samples do not exhibit significant enrichment or depletion of fluid mobile elements and have similar Sr-Nd-Pb isotope values compared to other unaffected samples (Choi et al., 2022). Furthermore, the $\delta^{18}O_{olvine}$ of the samples erupted underwater shows mantle-like $\delta^{18}O_{olvine}$ values, distinctly different from the $\delta^{18}O$ of altered basalts showing 10 to 20 ‰ typically seen in altered basalts (Eiler, 2001). Consequently, trace elements and Sr, Nd, Pb, and O isotopes in these samples remain unaffected by post-eruptive alteration, preserving their original compositions. However, since helium is a volatile element, its isotope ratio might be modified by diffusive helium loss and ^{4}He addition. This aspect will be further discussed in section 5.2.

5.2. Reliability evaluation of helium isotopes in the basalt samples

In this study, when we combine the new $^{3}He/^{4}He$ values of HT, JPH and BD with the existing helium isotope values (Kim et al., 2021; Lee et al., 2021), the $^{3}He/^{4}He$ ratios in the basalt rocks ranges from 3.5 to 7.3 R_a (Fig. 5). However, a careful evaluation of data reliability in order to accurately interpret this variability is necessary, as some JJ and UL samples with lower $^{3}He/^{4}He$ ratios than others may have been affected by degassing, diffusive helium loss, and/or radiogenic ^{4}He addition. Among them, the JJ sample exhibits the most variable $^{3}He/^{4}He$ ratio (3.5 to 7.3 R_a) in the study region. First, the DB-01, DB-02, and DB-03 samples have similar Sr-Nd-Pb isotope ratios indicating the same magma origin but showing variable $^{3}He/^{4}He$ ratios (5.6 to 7.3 R_a). The SB-01 sample has the lowest $^{3}He/^{4}He$ ratio with the highest helium concentration among the datasets, which, as observed in other environments with magmatism, exhibits helium isotopic disequilibrium among the crystal phases (Marty et al., 1994; Nuccio et al., 2008), partial helium (^{3}He, preferentially) loss from fluid inclusions (Burnard, 2004; Yamamoto et al., 2009), and/or the addition of radiogenic ^{4}He to fluid inclusions. For the UL samples, it also exhibits variable 3He/4He ratio (4.5 to 6.0 R_a). Clinopyroxene phenocrysts of UD-3 show the lowest helium concentration and the lowest $^{3}He/^{4}He$ ratio among the UL samples, suggesting the possibility of diffusive helium loss from fluid inclusions and consequent isotopic fractionation (Burnard, 2004; Yamamoto et al., 2009). Considering all of the above possible issues, the listed samples would prefer to be excluded from the following discussions about magma sources, as they undergo the occurrence of secondary processes or modifications during magma ascension within the volcanic plumbing system. In general, the most likely ranges of $^{3}He/^{4}He$ ratios for the basalts are as follows: HT: 6.8 to 7.3 R_a, JPH: 7.2 R_a, BD: higher than 5.3 R_a, JJ: 6.8 to 7.3 R_a, UL: 6 R_a, and DD: 5.7 to 5.9 R_a. Overall, the helium isotopic ratios of the basalts range from 5.7 to 7.3 R_a.

5.3. Magma sources

5.3.1. Source lithology

The variable trace element patterns in the Korean Peninsula basalt samples reflect both the mantle components and the degree of partial melting (Fig. 3b). We devise that the pyroxenite source is known to play an important role in the magma sources the most intraplate volcanoes (Sobolev et al., 2007; Yang et al., 2016). And, using the chemical markers of the pyroxenite contribution proposed by Yang et al. (2016), we defined the source properties and melting regime using the melting model of peridotite and pyroxenite in the La/Yb versus $FeO^{T}/CaO - 3*MgO/SiO_2$ (FC3MS) diagram. Furthermore, the association of the pyroxenite source in mantle components has been proposed by elevated FC3MS values in the La/Yb vs. FC3MS plots (Fig. 7). Using this, the UL samples are described as a mixture of garnet peridotite and pyroxenite, and the JJ and HT samples should have a pyroxenite source for the magma generation.

Since olivine is initially crystallized from basaltic magma (Sobolev et al., 2007), we put together olivine phenocryst geochemical data from previous studies (Choi et al., 2014; Choi et al., 2020; Choi et al., 2022; Kim et al., 2021; Lee et al., 2021; Sakuyama et al., 2014). Using this compiled dataset, the olivine phenocrysts in the JJ and HT samples follow a distinct fractionation crystallization tendency for pyroxenite and peridotite melting, while other samples lack distinct correlations (Fig. S12). Olivines in the JJ samples appear near the melting region of the pyroxenite source with 100Ca/Fe, 100Ni/Mg, and Ni/(Mg/Fe)/1000 versus 100*Mn/Fe ratios, while other samples exhibit a wide range of 100*Mn/Fe ratios, indicating more complex multiple lithological mantle sources (Fig. S13).

In order to specify the lithology of basalt sources, trace element modeling for partial melting of various mantle rocks was performed. Most basalt samples exhibit Ba, Pb, and Sr positive anomalies, with the HT samples exhibiting a K positive anomaly. To identify these features, particularly the trace element pattern of the basaltic cognates from DD, Park et al. (2022) proposed melting generated by mixing ~38% partial melting of hornblendite + spinel as the metasomatized SCLM and 0.5% partial melting of clinopyroxene mush in a ratio of 0.6:0.4. The DD and UL samples are well described by the proposed melt components mentioned above, while there is a limitation that the K and Pb anomalies in other regions are not. To address this, we used the trace element fractionation equations from Shaw (1970) (Fig. 8) to calculate partial melting values of garnet pyroxenite from Xu-Huai (Wang et al., 2016) from dikes intruded during the Cretaceous in Xu-Huai within the North China Block and spinel peridotite found in Hannuoba (Rudnick et al., 2004) and the Korean Peninsula (Choi et al., 2005). The partition coefficients for the individual minerals required for the calculation are provided in Table S3 (Elkins et al., 2008; Hart and Dunn, 1993; McKenzie and O'Nions, 1991; Yurimoto and Ohtani, 1992). In addition, we used the garnet pyroxenite melting mode (Cpx: Grt = 0.9: 0.1) and the spinel peridotite in the Hannuoba melting mode (Ol: Opx: Cpx: Sp = 0.05: -0.49 : 1.31: 0.13) based on (Salters, 1996). For the spinel peridotite component in the Korean Peninsula, the melt composition was calculated using the trace element content and partition coefficient of clinopyroxene. The results of the partial melting modeling are presented in Table S4. The melts of spinel peridotite exhibited a different range compared to the basalt samples, whereas the melts of garnet pyroxenite showed characteristic K and Pb anomalies (Fig. 8). The trace element patterns of the samples can be explained by the mixing of melts from hornblendite in the metasomatized SCLM and spinel peridotite with partial melts of the garnet pyroxenite.

5.3.2. Sr-Nd-Pb isotopes

The Sr-Nd-Pb isotope values of our basalt samples indicate that DMM, EM1, and EM2 components were all involved, as previously reported in the same study area (Chen et al., 2007; Choi et al., 2006). Notably, most basalts, except for the JJ samples, exhibit the presence of the EM1 component (Fig. 9). The JJ samples plot towards the EM2 end-member, suggesting a mixing between DMM and EM2 (Figs. 9b and c). The UL and DD samples plot in the DMM-EM1-EM2 mixing area (Fig. 9c). The isotopic signature of the basalts around the Korean Peninsula aligns with broader regional patterns observed in Northeast China, dominated by DMM-EM1 mixing, and Southeast Asia, characterized by DMM-EM2 influence, as reported by Choi et al. (2006).

Possible sources for EM1 and EM2 include the metasomatized SCLM and/or subducted sediments stored in the mantle transition zone (Kuritani et al., 2011; Tian et al., 2016; Yu et al., 2018). As discussed in the previous section, the concurrence of low $^{3}He/^{4}He$ ratios in the basalts and mantle xenoliths from the surrounding areas of the Korean Peninsula would indicate the SCLM-like contribution to the magma source. The isotopic distribution indicates a spatial boundary between the two mantle domains in East Asia. This constitutes a continuous boundary between the North China Block and the South China Block, and the isotopic differences between the two indicate that the enriched components represent the delaminated continental lithosphere (Park et al., 2005). The pyroxenite and amphibolite sources in the metasomatized SCLM could be EM1 and EM2 components for generating the basalts (Kim et al., 2021; Park et al., 2022). Moreover, the back-arc basin basalts of Yamato basin and Japan basin in the East Sea (Sea of Japan) have no EM1 signatures (Hirahara et al., 2015).

In contrast, following the opening of the back-arc basin, volcanoes located on the extended continental crust of the East Sea (Sea of Japan), including UL and DD, exhibit a mixing relationship of DMM-EM1-EM2 compositions (Lee et al., 2011; Morishita et al., 2020). This compositional difference between the back-arc basin basalts and the intraplate volcanoes in the East Sea (Sea of Japan) indicates that the SCLM could be responsible for the EM1 component. Consequently, the Sr-Nd-Pb isotopes together with the helium isotopes imply that the basalts were derived from heterogeneous mantle sources influenced by the metasomatized SCLM. The distinct isotopic signatures of EM1 and EM2 components in the basalts, especially the high $^{3}He/^{4}He$ ratios, suggest a significant contribution from the metasomatized SCLM, delineating a clear boundary between the mantle domains in East Asia and highlighting the role of the delaminated continental lithosphere in the magma source.

5.3.3 Oxygen isotopes

Most basalt samples ($\delta^{18}O_{olivine}$ = 5.1 to 5.7 ‰), except for the JJ basalts, have similar and slightly higher $\delta^{18}O$ values than the MORB range ($\delta^{18}O_{olivine}$ = 5.1 ± 0.2 ‰, Eiler, 2001). In contrast, the JJ basalts have lower $\delta^{18}O$ values ($\delta^{18}O_{olivine}$ = 4.7 to 5.1 ‰) than the MORB range despite containing the EM2 component (Fig. 4 and 8, Choi et al., 2006). It is known that low $\delta^{18}O$ values can be attributed to water-rock interaction at high temperatures, and hydrothermally altered lower oceanic crust has low $\delta^{18}O$ values (Eiler et al., 1997; Hart et al., 1999; Wang et al., 2011; Wang et al., 2015; Zhang et al., 2009). The JJ basalts with low $\delta^{18}O$ olivine values have high FC3MS (Yang et al., 2016) values (> 0.7), indicating a contribution from the pyroxenite source formed by the interaction between subducted oceanic crust and the mantle (Fig. S14b). The olivine phenocryst chemistry of the JJ basalts also shows a more distinct pyroxenite source compared to other basalt samples. It has been suggested that the origin of pyroxenite with low $\delta^{18}O$ values is derived from the altered SCLM through ancient subduction processes (Wang et al., 2011; Zhang et al., 2009). Using this, we propose that the low $\delta^{18}O$ values observed in some basalt samples are determined to reflect these differences in lithology.

5.3.4. Helium isotopes

All of the basalt samples show lower $^{3}He/^{4}He$ ratios (5.7 to 7.3 R_a) than the MORB range (7 to 9 R_a). As suggested in previous sections, subducted sediments and the SCLM could be potential causes of lowering the $^{3}He/^{4}He$ ratios. Subducted sediments with relatively abundant U and Th contents, can reduce the $^{3}He/^{4}He$ ratios in slab fluids, which are ultimately degassed during arc volcanism (Rizzo et al., 2022). However, the maximum $^{3}He/^{4}He$ ratios observed in volcanic fumaroles in Japan, located at the arc front and significantly influenced by slab fluids, are ~7.5 R_a (Sano and Marty, 1995) which is higher than that observed in the basalts. Additionally, over 90% of ^{4}He produced by the alpha decay of U and Th within recycled materials is diffused into the surrounding asthenospheric mantle due to the high diffusivity of helium (Hart et al., 2008). Moreover, it has been reported that diamonds generated in the mantle transition zone have carbon isotopic components ($\delta^{13}C$ = -2.7 to -26 ‰) derived from recycled pelagic sediments, exhibiting higher $^{3}He/^{4}He$ ratios (up to 49.9 R_a) than DMM (Timmerman et al., 2019). Likewise, many OIBs with enriched radiogenic isotopes exhibit the DMM-like $^{3}He/^{4}He$ ratios (e.g., Pitcairn Island, the Malu trend of Samoan volcanic lineaments, and the North Fiji Basin, Fig. S15, Garapić et al., 2015; Jackson et al., 2014; Oh et al., 2021). Consequently, subducted sediments are unlikely to be the primary source of the low $^{3}He/^{4}He$ ratios observed in our basalts.

Another potential source of the low $^{3}He/^{4}He$ ratio is the SCLM, which is characterized by $^{3}He/^{4}He$ of 6.1±0.9 R_a (Gautheron and Moreira, 2002). The SCLM beneath East Asia, including the Korean Peninsula, was metasomatized by the subduction of the Izanagi and Pacific plates before the back-arc basin opening (Chen et al., 2007; Kim et al., 2005; Yu et al., 2018; Zhang et al., 2009). It has been reported that pyroxenite and eclogite in the cratonic SCLM have more enriched Pb isotopes and lower $^{3}He/^{4}He$ ratios than the typical SCLM (Day et al., 2015). The $^{3}He/^{4}He$ ratios of the SCLM beneath the Korean Peninsula were suggested < 0.2 R_a to 7.7 R_a (Kim et al., 2005). The xenolith samples from Baekryungdo (XBR) with a low $^{3}He/^{4}He$ ratio (<0.2 R_a) have lower ^{4}He concentrations compared with other samples indicating diffusive loss of helium. Therefore, the $^{3}He/^{4}He$ ratios of the SCLM beneath the Korean Peninsula range from 4.6 to 7.7 R_a, when considering only samples analyzed by crushing except the XBR samples, which is similar to the SCLM beneath NE China (5 to 7 R_a) (Chen et al., 2007; Kim et al., 2005). The basalts overlap the range of $^{3}He/^{4}He$ values measured in mantle xenoliths from the Korean Peninsula (4.6 to 7.7 R_a) and NE China (5 to 7 R_a), suggesting the SCLM-like signature of helium isotopic ratio. Cratonic delamination beneath East Asia, which occurred approximately at 135 Ma, possibly subsequently involved as an enriched source (Liu et al., 2019). The cratonic SCLM is also observed beneath the Korean Peninsula through mantle tomography and mantle xenoliths (Samuel et al., 2023; Song et al., 2020). The remnant or delaminated SCLM could contribute to the source of the magma as well as a lower than MORB $^{3}He/^{4}He$ signature.

Since helium behaves as an incompatible element ($^{ol/melt}D_{He}$: 0.00017±13 and $^{cpx/melt}D_{He}$: 0.0002±2), with almost negligible differences among its two isotopes (D_{3He}/D_{4He}) (Burnard, 2004; Heber et al., 2007; Rizzo et al., 2018), the $^{3}He/^{4}He$ variability can only be interpreted in terms of mantle heterogeneity. The La/Nb ratio is distinctly differentiated between peridotite and pyroxenite sources due to differences in their partition coefficients, regardless of the degree of partial melting (Stracke and Bourdon, 2009). The variable La/Yb ratios of the peridotite and pyroxenite melts represent that the La/Yb ratios of melts are affected by the source enrichment and degree of partial melting. All samples have low La/Nb ratios and variable La/Yb ratios

with enriched $^{143}Nd/^{144}Nd$ ratios which indicate an enriched pyroxenite source. The high La/Yb and low $^{3}He/^{4}He$ ratios in basalts suggest a significant involvement of an enriched mantle component characterized by the presence of the SCLM in the magma source (Chen et al., 2023; Dodson et al., 1998; Lee et al., 2021). Most samples have La/Nb and La/Yb ratios and low $^{3}He/^{4}He$ ratios within the pyroxenite melt range (Fig. 10c and d). The UL and DD samples, which have more enriched $^{143}Nd/^{144}Nd$ isotopes and higher La/Yb ratios, also exhibit lower $^{3}He/^{4}He$ ratios (Fig. 10d and e). Therefore, the low $^{3}He/^{4}He$ ratios in the basalts with low La/Nb ratios, variable La/Yb ratios, and enriched $^{143}Nd/^{144}Nd$ ratios, suggest an enriched pyroxenite source in the SCLM.

5.4. Geodynamic implications for the mantle beneath Northeast Asia

UL and DD (5.7 to 6.0 R_a) have lower $^{3}He/^{4}He$ ratios compared to other basalts (HT, JPH, and JJ; ~7.3 R_a) located in the continental margin. UL and DD experienced more extensive extensional activity compared to other volcanoes (HT, JPH, and JJ) in the continental margin due to the opening of the East Sea (Sea of Japan). According to the numerical modeling, lithospheric delamination can occur during the opening of back-arc basins (Göğüş and Ueda, 2018). This phenomenon has been observed at Kueishantao, located at the tectonic junction of the southernmost part of the Okinawa Trough, indicating delamination in an actively extending back-arc basin (Guo et al., 2022). In the East Sea (Sea of Japan), such delamination would have facilitated enhanced lithosphere-asthenosphere interaction, likely resulting in the low $^{3}He/^{4}He$ isotope ratios of UL and DD. The current mantle tomography studies have not confirmed the presence of the delaminated SCLM beneath the East Sea (Sea of Japan) (Lee et al., 2022; Liang et al., 2022). This may be due to the sparse installation of seismometers in the area, leading to lower resolution in tomography that hinders the detection of such features. The remnant and/or delaminated SCLM could involve the source of the magma as well as low $^{3}He/^{4}He$ reservoirs.

Thus, we derived a mixing model to evaluate how much each enrichment process influenced the magma formation. The helium and radiogenic isotope ratios and the quantities of each end-member are shown in Table S5. We assumed that the EM1 and EM2 sources originated from the SCLM and had low $^{3}He/^{4}He$ ratios to explain the enriched basalts with low $^{3}He/^{4}He$ ratios. According to the mixing model, the mixing line in the He and radiogenic isotope diagram shows that for the sample, about 5 to 30% of the EM1 and EM2 with the SCLM-like $^{3}He/^{4}He$ signature was involved in magma formation (Fig. 11). The lithosphere-asthenosphere interaction plays a significant role in magma genesis, as evidenced by the low $^{3}He/^{4}He$ ratios of the basalts from Tengchong volcano, SE Tibet and Tertiary basalts of the western USA (Chen et al., 2023; Dodson et al., 1998). Variable structures of the lithospheric mantle and complex small-scale circulation of the asthenosphere are observed in the Korean Peninsula and Northeast China regions (Song et al., 2020; Zhang et al., 2021). This heterogeneous lithospheric mantle structure, including the reactivation of the cratonic margin, indicates a dynamic interaction between the mantle and the SCLM.

The mixing between the enriched sources in the remnant cratonic or delaminated SCLM and DMM could explain the distribution in the He and radiogenic isotope plots of the basalts. The spinel peridotite mantle xenoliths found in the Cenozoic volcanics of the Korean Peninsula are depleted, whereas the pyroxenite within the SCLM exhibits enriched characteristics such as

low $\delta^{26}Mg$ and high $^{87}Sr/^{86}Sr$ ratios with high water contents (Azevedo-Vannson et al., 2021; Choi et al., 2005; Wang et al., 2016). The interaction between pyroxenite, which exists as remnants or delaminated fragments within the cratonic SCLM, and the peridotite of DMM can generate the magma responsible for the Cenozoic intraplate volcanism in Northeast Asia (Fig. 12). In summary, the Sr, Nd, Pb, and O isotopes of the basalts from the surrounding Korean Peninsula represent a heterogeneous enriched magma source. Integrating helium isotope data with major and trace elements, and radiogenic isotopes (Sr, Nd, and Pb) shows that the enriched sources originated from the pyroxenite in metasomatized SCLM.

6. Conclusions

In this study, the He-Sr-Nd-Pb-O isotope compositions of the basalts around the Korean Peninsula elucidate the upper mantle scale enrichment that caused Cenozoic intraplate volcanism in Northeast Asia. Measure $^{3}He/^{4}He$ ratios of our basalt samples range from 5.7 to 7.3 R_a. $^{3}He/^{4}He$ values lower than 5.7 Ra are attributed to secondary processes and/or post-magmatic addition of radiogenic ^{4}He. Using major and trace elements to identify source lithology, we found that the JJ samples are mostly derived from the pyroxenite source, while other samples have a complex mixed origin of peridotite and pyroxenite sources. The presence of hornblendite and garnet pyroxenite in the metasomatized SCLM can explain the K, Sr, and Pb positive anomalies observed in the samples. Based on Sr, Nd, and Pb isotopes, except for the JJ samples, the basalts exhibit the EM1 contribution. The JJ samples plot towards the EM2 end-member, displaying a mixing relationship between DMM and EM2. Although most of the basalt samples have DMM-like $\delta^{18}O$ values ($\delta^{18}O_{olivine}$ = 5.1 to 5.7 ‰), the JJ basalts have lower $\delta^{18}O$ values ($\delta^{18}O_{olivine}$ = 4.7 to 5.1 ‰) than the MORB range, indicating a contribution from the pyroxenite source formed by the interaction between subducted oceanic crust and the DMM component. The low $^{3}He/^{4}He$ ratios, along with low La/Nb, high La/Yb, and low $^{143}Nd/^{144}Nd$ ratios, imply that the enriched pyroxenite source in the remnant or delaminated SCLM could contribute to the magma generation instead of subducted sediments stored in the MTZ. Geodynamically, the delaminated cratonic SCLM and its interaction with the asthenosphere could decrease the $^{3}He/^{4}He$ ratios of the basalts, particularly UD and DD. Furthermore, it is shown that approximately 5 to 30% of the EM1 and EM2 components with the SCLM-like sources might be involved in magmatism. Therefore, our findings suggest that the SCLM is the significant source that caused the geochemically enriched properties of the Cenozoic intraplate magmatism in Northeast Asia.

Declaration of competing interest

The authors declare that they have no known competing financial interests or personal relationships that could have appeared to influence the work reported in this paper.

Acknowledgments

This study was sponsored by the National Research Foundation of Korea (NRF) grant funded by the Ministry of Science and ICT (2022R1C1C1007104 and 2022R1A5A1085103). This work was also supported by the Ministry of Oceans and Fisheries of Korea (grant no. PG53500). The Authors are grateful to Mariano Tantillo and Mariagrazia Misseri for helping in sample preparation and during the isotope analysis of noble gases.

7. References

Azevedo-Vannson, S., France, L., Ingrin, J., Chazot, G., 2021. Mantle metasomatic influence on water contents in continental lithosphere: New constraints from garnet pyroxenite xenoliths (France & Cameroon volcanic provinces). Chem. Geol. 575.

Burnard, P., 2004. Diffusive fractionation of noble gases and helium isotopes during mantle melting. Earth Planet. Sci. Lett. 220, 287-295.

Chen, K., He, H., Stuart, F., Liu, S., Xu, X., Cheng, Z., Yang, D., Li, J., Su, F., Wang, W., 2023. Binary mixing of lithospheric mantle and asthenosphere beneath Tengchong volcano, SE Tibet: evidence from noble gas isotopic signatures. Int. Geol. Rev. 65, 236-252.

Chen, Y., Zhang, Y., Graham, D., Su, S., Deng, J., 2007. Geochemistry of Cenozoic basalts and mantle xenoliths in Northeast China. Lithos 96, 108-126.

Cho, M., Lee, Y., Kim, T., Cheong, W., Kim, Y., Lee, S.R., 2017. Tectonic evolution of Precambrian basement massifs and an adjoining fold-and-thrust belt (Gyeonggi Marginal Belt), Korea: An overview. Geosci. J. 21, 845-865.

Choi, H.-O., Choi, S.H., Yu, Y., 2014. Isotope geochemistry of Jeongok basalts, northernmost South Korea: Implications for the enriched mantle end-member component. J. Asian Earth Sci.91, 56-68.

Choi, H.-O., Choi, S.H., Lee, Y.S., Ryu, J.-S., Lee, D.-C., Lee, S.-G., Sohn, Y.K., Liu, J.-q., 2020. Petrogenesis and mantle source characteristics of the late Cenozoic Baekdusan (Changbaishan) basalts, North China Craton. Gondwana Res. 78, 156-171.

Choi, H.-O., Kim, J., Oh, J., Kim, C.H., Choi, S.Y., Kim, W.H., Park, C.H., 2022. Petrogenesis of submarine volcanic rocks dredged from Dokdo, Ulleungdo, and the neighboring seamounts in the East Sea: Constraints from mineral chemistry, geochemistry, and $^{40}Ar/^{39}Ar$ ages. Lithos 426-427.

Choi, S.H., Kwon, S.-T., Mukasa, S.B., Sagong, H., 2005. Sr–Nd–Pb isotope and trace element systematics of mantle xenoliths from Late Cenozoic alkaline lavas, South Korea. Chem. Geol. 221, 40-64.

Choi, S.H., Mukasa, S.B., Kwon, S.-T., Andronikov, A.V., 2006. Sr, Nd, Pb and Hf isotopic compositions of late Cenozoic alkali basalts in South Korea: Evidence for mixing between the two dominant asthenospheric mantle domains beneath East Asia. Chem. Geol. 232, 134-151.

Choi, S.H., 2021. Geochemistry and petrogenesis of Quaternary volcanic rocks from Ulleung Island, South Korea. Lithos 380-381.

Chough, S.K., Kwon, S.T., Ree, J.H., Choi, D.K., 2000. Tectonic and sedimentary evolution of the Korean peninsula: a review and new view. Earth-Sci. Rev. 52, 175-235.

Danyushevsky, L.V., Plechov, P., 2011. Petrolog3: Integrated software for modeling crystallization processes. Geochem. Geophys. Geosyst. 12, n/a-n/a.

Day, J.M.D., Barry, P.H., Hilton, D.R., Burgess, R., Pearson, D.G., Taylor, L.A., 2015. The helium flux from the continents and ubiquity of low-3He/4He recycled crust and lithosphere. Geochim. Cosmochim. Acta 153, 116-133.

Dodson, A., DePaolo, D.J., Kennedy, B.M., 1998. Helium isotopes in lithospheric mantle: evidence from tertiary basalts of the western USA. Geochim. Cosmochim. Acta 62, 3775-3787.

Dygert, N., Liang, Y., Hess, P., 2013. The importance of melt TiO2 in affecting major and trace element partitioning between Fe–Ti oxides and lunar picritic glass melts. Geochim. Cosmochim. Acta 106, 134-151.

Eiler, J.M., Farley, K.A., Valley, J.W., Hauri, E., Craig, H., Hart, S.R., Stolper, E.M., 1997. Oxygen isotope variations in ocean island basalt phenocrysts. Geochim. Cosmochim. Acta 61, 2281-2293.

Eiler, J.M., 2001. Oxygen isotope variations of basaltic lavas and upper mantle rocks. Rev. Mineral. Geochem.43, 319-364.

Elkins, L.J., Gaetani, G.A., Sims, K.W.W., 2008. Partitioning of U and Th during garnet pyroxenite partial melting: Constraints on the source of alkaline ocean island basalts. Earth Planet. Sci. Lett. 265, 270-286.

Garapić, G., Jackson, M.G., Hauri, E.H., Hart, S.R., Farley, K.A., Blusztajn, J.S., Woodhead, J.D., 2015. A radiogenic isotopic (He-Sr-Nd-Pb-Os) study of lavas from the Pitcairn hotspot: Implications for the origin of EM-1 (enriched mantle 1). Lithos 228-229, 1-11.

Gautheron, C., Moreira, M., 2002. Helium signature of the subcontinental lithospheric mantle. Earth Planet. Sci. Lett. 199, 39-47.

Göğüş, O.H., Ueda, K., 2018. Peeling back the lithosphere: Controlling parameters, surface expressions and the future directions in delamination modeling. J. Geodyn. 117, 21-40.

Gonnermann, H.M., Mukhopadhyay, S., 2009. Preserving noble gases in a convecting mantle. Nature 459, 560-563.

Graham, D.W., 2002. Noble gas isotope geochemistry of mid-ocean ridge and ocean island basalts: Characterization of mantle source reservoirs. Rev. Mineral. Geochem.47, 247-317.

Guo, J., Guo, F., Wang, C.Y., Li, C., 2013. Crustal recycling processes in generating the early Cretaceous Fangcheng basalts, North China Craton: New constraints from mineral chemistry, oxygen isotopes of olivine and whole-rock geochemistry. Lithos 170, 1-16.

Guo, K., Wang, X., Chen, S., Shang, L., Liu, B., Zhang, X., Lai, Z., 2022. The delamination of lower crust in continental back-arc basin: Evidence from Sr isotope and elemental compositions of plagioclase and clinopyroxene in andesites from Kueishantao, north of Taiwan, China. Lithos 416, 106653.

Hart, S.R., Dunn, T., 1993. Experimental cpx/melt partitioning of 24 trace elements. Contrib. Mineral. Petrol. 113, 1-8.

Hart, S.R., Blusztajn, J., Dick, H.J., Meyer, P.S., Muehlenbachs, K., 1999. The fingerprint of seawater circulation in a 500-meter section of ocean crust gabbros. Geochim. Cosmochim. Acta 63, 4059-4080.

Hart, S.R., Kurz, M.D., Wang, Z., 2008. Scale length of mantle heterogeneities: Constraints from helium diffusion. Earth Planet. Sci. Lett. 269, 508-517.

Hawkesworth, C.J., Norry, M.J., Roddick, J.C., Vollmer, R., 1979. 143Nd/144Nd and 87Sr/86Sr ratios from the Azores and their significance in LIL-element enriched mantle. Nature 280, 28-31.

Hawkesworth, C.J., Kempton, P.D., Rogers, N.W., Ellam, R.M., van Calsteren, P.W., 1990. Continental mantle lithosphere, and shallow level enrichment processes in the Earth's mantle. Earth Planet. Sci. Lett. 96, 256-268.

Heber, V.S., Brooker, R.A., Kelley, S.P., Wood, B.J., 2007. Crystal–melt partitioning of noble gases (helium, neon, argon, krypton, and xenon) for olivine and clinopyroxene. Geochim. Cosmochim. Acta 71, 1041-1061.

Hirahara, Y., Kimura, J.I., Senda, R., Miyazaki, T., Kawabata, H., Takahashi, T., Chang, Q., Vaglarov, B.S., Sato, T., Kodaira, S., 2015. Geochemical variations in Japan Sea back-arc basin basalts formed by high-temperature adiabatic melting of mantle metasomatized by sediment subduction components. Geochem. Geophys. Geosyst. 16, 1324-1347.

Hofmann, A.W., White, W.M., 1982. Mantle plumes from ancient oceanic crust. Earth Planet. Sci. Lett. 57, 421-436.

Hofmann, A.W., Jochum, K.P., Seufert, M., White, W.M., 1986. Nb and Pb in oceanic basalts: new constraints on mantle evolution. Earth Planet. Sci. Lett. 79, 33-45.

Hofmann, A.W., 2003. Sampling Mantle Heterogeneity through Oceanic Basalts: Isotopes and Trace Elements. Treatise on Geochemistry 2, 568.

Jackson, M.G., Hart, S.R., Konter, J.G., Kurz, M.D., Blusztajn, J., Farley, K.A., 2014. Helium and lead isotopes reveal the geochemical geometry of the Samoan plume. Nature 514, 355-358.

Kim, D., Lee, H., Lee, W., Kim, J., Oh, J., Song, J.-H., Jung, H., Stuart, F.M., 2021. Helium isotopes and olivine geochemistry of basalts and mantle xenoliths in Jeju Island, South Korea: Evaluation of role of SCLM on the Cenozoic intraplate volcanism in East Asia. Lithos 390, 106123.

Kim, J.-I., Choi, S.H., Koh, G.W., Park, J.B., Ryu, J.-S., 2019a. Petrogenesis and mantle source characteristics of volcanic rocks on Jeju Island, South Korea. Lithos 326, 476-490.

Kim, K.H., Nagao, K., Tanaka, T., Sumino, H., Nakamura, T., Okuno, M., Lock, J.B., Youn, J.S., Song, J., 2005. He-Ar and Nd-Sr isotopic compositions of ultramafic xenoliths and host alkali basalts from the Korean peninsula. Geochem. J. 39, 341-356.

Kim, N.K., Kusakabe, M., Park, C., Lee, J.I., Nagao, K., Enokido, Y., Yamashita, S., Park, S.Y., 2019b. An automated laser fluorination technique for high-precision analysis of three oxygen isotopes in silicates. Rapid Commun. Mass Spectrom. 33, 641-649.

Kim, Y., Lee, C., Kim, S.-S., 2015. Tectonics and volcanism in East Asia: Insights from geophysical observations. J. Asian Earth Sci.113, 842-856.

Koh, G.W., Park, J.B., Kang, B.-R., Kim, G.-P., Moon, D.C., 2013. Volcanism in Jeju Island. J. Geol. Soc. Korea 49, 209-230.

Kuritani, T., Ohtani, E., Kimura, J.-I., 2011. Intensive hydration of the mantle transition zone beneath China caused by ancient slab stagnation. Nat. Geosci. 4, 713-716.

Kurz, M.D., Jenkins, W.J., Hart, S.R., 1982. Helium isotopic systematics of oceanic islands and mantle heterogeneity. Nature 297, 43-47.

Le Bas, M.J., Maitre, R.W.L., Streckeisen, A., Zanettin, B., Rocks, IUGS Subcommission on the Systematics of Igneous Rocks, 1986. A chemical classification of volcanic rocks based on the total alkali-silica diagram. J. Petrol. 27, 745-750.

Lee, J.-A., Kim, K., Lee, J.-I., Choo, M., 2013. Oxygen Isotopic Ratios for Ultramafic Xenoliths from the Korean Peninsula. Journal of the Korean earth science society 34, 28-40.

Lee, M.J., Lee, J.I., Kwon, S.-T., Choo, M.K., Jeong, K.-S., Cho, J.-H., Kim, S.-R., 2011. Sr-Nd-Pb isotopic compositions of submarine alkali basalts recovered from the South Korea Plateau, East Sea. Geosci. J. 15, 149-160.

Lee, M.J., Lee, J.I., Kim, T.H., Lee, J., Nagao, K., 2015. Age, geochemistry and Sr-Nd-Pb isotopic compositions of alkali volcanic rocks from Mt. Melbourne and the western Ross Sea, Antarctica. Geosci. J. 19, 681-695.

Lee, S., Saxena, A., Song, J.-H., Rhie, J., Choi, E., 2022. Contributions from lithospheric and upper-mantle heterogeneities to upper crustal seismicity in the Korean Peninsula. Geophys. J. Int. 229, 1175-1192.

Lee, S.H., Oh, C.W., Cho, D.-L., Lee, B.C., Lee, B.Y., 2023. Early Cretaceous magmatism in the northern Gyeonggi Massif and the northcentral Yeongnam Massif, Korean Peninsula: Its implications for the Cretaceous tectonic evolution of the Northeast Asia. Lithos 460, 107366.

Lee, W., Lee, H., Kim, D., Kim, J., Oh, J., Song, J.-H., Kim, C.H., Park, C.H., Stuart, F.M., 2021. Trace element and helium isotope geochemistry of the Cenozoic intraplate volcanism in the East Sea (Sea of Japan): Implications for lithosphere-asthenosphere interaction. Lithos 388, 106075.

Liang, X., Zhao, D., Xu, Y.G., Hua, Y., 2022. Anisotropic tomography and dynamics of the big mantle wedge. Geophys. Res. Lett. 49, e2021GL097550.

Liu, J., Cai, R., Pearson, D.G., Scott, J.M., 2019. Thinning and destruction of the lithospheric mantle root beneath the North China Craton: A review. Earth-Sci. Rev. 196, 102873.

Marty, B., Trull, T., Lussiez, P., Basile, I., Tanguy, J.-C., 1994. He, Ar, O, Sr and Nd isotope constraints on the origin and evolution of Mount Etna magmatism. Earth Planet. Sci. Lett. 126, 23-39.

McKenzie, D., O'Nions, R.K., 1991. Partial Melt Distributions from Inversion of Rare Earth Element Concentrations. J. Petrol. 32, 1021-1091.

Morishita, T., Hirano, N., Sumino, H., Sato, H., Shibata, T., Yoshikawa, M., Arai, S., Nauchi, R., Tamura, A., 2020. Alkali basalt from the Seifu Seamount in the Sea of Japan: post-spreading magmatism in a back-arc setting. Solid Earth 11, 23-36.

Nardini, I., Armienti, P., Rocchi, S., Dallai, L., Harrison, D., 2009. Sr–Nd–Pb–He–O Isotope and Geochemical Constraints on the Genesis of Cenozoic Magmas from the West Antarctic Rift. J. Petrol. 50, 1359-1375.

Nuccio, P.M., Paonita, A., Rizzo, A., Rosciglione, A., 2008. Elemental and isotope covariation of noble gases in mineral phases from Etnean volcanics erupted during 2001–2005, and genetic relation with peripheral gas discharges. Earth Planet. Sci. Lett. 272, 683-690.

Oh, J., Lee, I., Stuart, F.M., Park, M., Kim, J., 2021. EM1-Signature in the North Fiji Basin: Evidence for Stagnant Slab-Derived Mantle Upwelling Beneath the Trench-Distal Back-Arc Basin. J. Geophys. Res. Solid Earth126, e2020JB021017.

Ozima, M., Podosek, F.A., 2002. Noble Gas Geochemistry, 2 ed. Cambridge University Press, Cambridge.

Park, J., Lim, H., Myeong, B., Jang, Y.-D., Brenna, M., 2022. Basaltic cognate enclaves from Dokdo Island as a window for intraplate mafic alkaline OIB magma dynamics in a back-arc basin. Contrib. Mineral. Petrol. 177, 86.

Park, K.-H., Park, J.-B., Cheong, C.-S., Oh, C.W., 2005. Sr, Nd and Pb isotopic systematics of the Cenozoic basalts of the Korean Peninsula and their implications for the Permo-Triassic continental collision boundary. Gondwana Res. 8, 529-538.

Pilet, S., Baker, M.B., Stolper, E.M., 2008. Metasomatized Lithosphere and the Origin of Alkaline Lavas. Science 320, 916-919.

Rizzo, A.L., Pelorosso, B., Coltorti, M., Ntaflos, T., Bonadiman, C., Matusiak-Małek, M., Italiano, F., Bergonzoni, G., 2018. Geochemistry of noble gases and CO2 in fluid inclusions from lithospheric mantle beneath Wilcza Góra (Lower Silesia, Southwest Poland). Front. Earth Sci. 6, 215.

Rizzo, A.L., Robidoux, P., Aiuppa, A., Di Piazza, A., 2022. 3He/4He Signature of Magmatic Fluids from Telica (Nicaragua) and Baru (Panama) Volcanoes, Central American Volcanic Arc. Appl. Sci. 12, 4241.

Rudnick, R.L., Gao, S., 2003. 3.01 - Composition of the Continental Crust, In: Holland, H.D., Turekian, K.K. (Eds.), Treatise on Geochemistry. Pergamon, Oxford, pp. 1-64.

Rudnick, R.L., Gao, S., Ling, W.-l., Liu, Y.-s., McDonough, W.F., 2004. Petrology and geochemistry of spinel peridotite xenoliths from Hannuoba and Qixia, North China craton. Lithos 77, 609-637.

Ryu, S., Oka, M., Yagi, K., Sakuyama, T., Itaya, T., 2011. K-Ar ages of the Quaternary basalts in the Jeongok area, the central part of Korean Peninsula. Geosci. J. 15, 1-8.

Sakuyama, T., Nagaoka, S., Miyazaki, T., Chang, Q., Takahashi, T., Hirahara, Y., Senda, R., Itaya, T., Kimura, J.i., Ozawa, K., 2014. Melting of the Uppermost Metasomatized Asthenosphere Triggered by Fluid Fluxing from Ancient Subducted Sediment: Constraints from the Quaternary Basalt Lavas at Chugaryeong Volcano, Korea. J. Petrol. 55, 499-528.

Salters, V.J.M., 1996. The generation of mid-ocean ridge basalts from the Hf and Nd isotope perspective. Earth Planet. Sci. Lett. 141, 109-123.

Samuel, V.O., Kwon, S., Jang, Y., Kil, Y., Santosh, M., Park, C., Yi, K., 2023. Fertile upper mantle peridotite xenoliths indicate no wholesale destruction of cratonic root in East Asia. Commun. Earth Environ. 4, 492.

Sano, Y., Marty, B., 1995. Origin of carbon in fumarolic gas from island arcs. Chem. Geol. 119, 265-274.

Shaw, D.M., 1970. Trace element fractionation during anatexis. Geochim. Cosmochim. Acta 34, 237-243.

Sobolev, A.V., Hofmann, A.W., Kuzmin, D.V., Yaxley, G.M., Arndt, N.T., Chung, S.-L., Danyushevsky, L.V., Elliott, T., Frey, F.A., Garcia, M.O., Gurenko, A.A., Kamenetsky, V.S., Kerr, A.C., Krivolutskaya, N.A., Matvienkov, V.V., Nikogosian, I.K., Rocholl, A., Sigurdsson, I.A., Sushchevskaya, N.M., Teklay, M., 2007. The Amount of Recycled Crust in Sources of Mantle-Derived Melts. Science 316, 412-417.

Son, M., Song, C.W., Kim, M.C., Cheon, Y., Cho, H., Sohn, Y.K., 2015. Miocene tectonic evolution of the basins and fault systems, SE Korea: dextral, simple shear during the East Sea (Sea of Japan) opening. J. Geol. Soc. 172, 664-680.

Song, J.-H., Kim, S., Rhie, J., 2020. Heterogeneous modification and reactivation of a craton margin beneath the Korean Peninsula from teleseismic travel time tomography. Gondwana Res. 81, 475-489.

Stracke, A., Bourdon, B., 2009. The importance of melt extraction for tracing mantle heterogeneity. Geochim. Cosmochim. Acta 73, 218-238.

Stuart, F.M., Lass-Evans, S., Godfrey Fitton, J., Ellam, R.M., 2003. High 3He/4He ratios in picritic basalts from Baffin Island and the role of a mixed reservoir in mantle plumes. Nature 424, 57-59.

Sun, C., Graff, M., Liang, Y., 2017. Trace element partitioning between plagioclase and silicate melt: The importance of temperature and plagioclase composition, with implications for terrestrial and lunar magmatism. Geochim. Cosmochim. Acta 206, 273-295.

Sun, S.-s., McDonough, W.F., 1989. Chemical and isotopic systematics of oceanic basalts: implications for mantle composition and processes. Geol. Soc. Lond. Spec. Publ. 42, 313-345.

Tamaki, K., 1995. Opening Tectonics of the Japan Sea, In: Taylor, B. (Ed.), Backarc Basins: Tectonics and Magmatism. Springer US, Boston, MA, pp. 407-420.

Tian, H.-C., Yang, W., Li, S.-G., Ke, S., Chu, Z.-Y., 2016. Origin of low δ26Mg basalts with EM-I component: Evidence for interaction between enriched lithosphere and carbonated asthenosphere. Geochim. Cosmochim. Acta 188, 93-105.

Timmerman, S., Honda, M., Burnham, A., Amelin, Y., Woodland, S., Pearson, D.G., Jaques, A., Le Losq, C., Bennett, V., Bulanova, G., 2019. Primordial and recycled helium isotope signatures in the mantle transition zone. Science 365, 692-694.

Wang, X.C., Wilde, S.A., Li, Q.L., Yang, Y.N., 2015. Continental flood basalts derived from the hydrous mantle transition zone. Nat. Commun. 6, 7700.

Wang, Y., Zhao, Z.-F., Zheng, Y.-F., Zhang, J.-J., 2011. Geochemical constraints on the nature of mantle source for Cenozoic continental basalts in east-central China. Lithos 125, 940-955.

Wang, Z.-Z., Liu, S.-A., Ke, S., Liu, Y.-C., Li, S.-G., 2016. Magnesium isotopic heterogeneity across the cratonic lithosphere in eastern China and its origins. Earth Planet. Sci. Lett. 451, 77-88.

Wang, Z., Liu, L., Fu, Y., Zhao, L., Lin, J., Jin, Z., Zheng, B., 2023. Multistage plate subduction controls intraplate volcanism and cratonic lithospheric thinning in Northeast Asia. Earth-Sci. Rev. 246.

Yamamoto, J., Nishimura, K., Sugimoto, T., Takemura, K., Takahata, N., Sano, Y., 2009. Diffusive fractionation of noble gases in mantle with magma channels: Origin of low He/Ar in mantle-derived rocks. Earth Planet. Sci. Lett. 280, 167-174.

Yang, Z.-F., Li, J., Liang, W.-F., Luo, Z.-H., 2016. On the chemical markers of pyroxenite contributions in continental basalts in Eastern China: Implications for source lithology and the origin of basalts. Earth-Sci. Rev. 157, 18-31.

Yoon, S.H., Sohn, Y.K., Chough, S.K., 2014. Tectonic, sedimentary, and volcanic evolution of a back-arc basin in the East Sea (Sea of Japan). Mar. Geol. 352, 70-88.

Yu, S.-Y., Xu, Y.-G., Zhou, S.-H., Lan, J.-B., Chen, L.-M., Shen, N.-P., Zhao, J.-X., Feng, Y.-X., 2018. Late Cenozoic basaltic lavas from the Changbaishan-Baoqing Volcanic Belt, NE China: Products of lithosphere-asthenosphere interaction induced by subduction of the Pacific plate. J. Asian Earth Sci.164, 260-273.

Yurimoto, H., Ohtani, E., 1992. Element partitioning between majorite and liquid: A secondary ion mass spectrometric study. Geophys. Res. Lett. 19, 17-20.

Zhang, A., Guo, Z., Afonso, J.C., Handley, H., Dai, H., Yang, Y., Chen, Y.J., 2021. Lithosphere–asthenosphere interactions beneath northeast China and the origin of its intraplate volcanism. Geology 50, 210-215.

Zhang, J.-J., Zheng, Y.-F., Zhao, Z.-F., 2009. Geochemical evidence for interaction between oceanic crust and lithospheric mantle in the origin of Cenozoic continental basalts in east-central China. Lithos 110, 305-326.

Zindler, A., Hart, S., 1986. Chemical Geodynamics. Annu. Rev. Earth Planet. Sci. 14, 493-571.

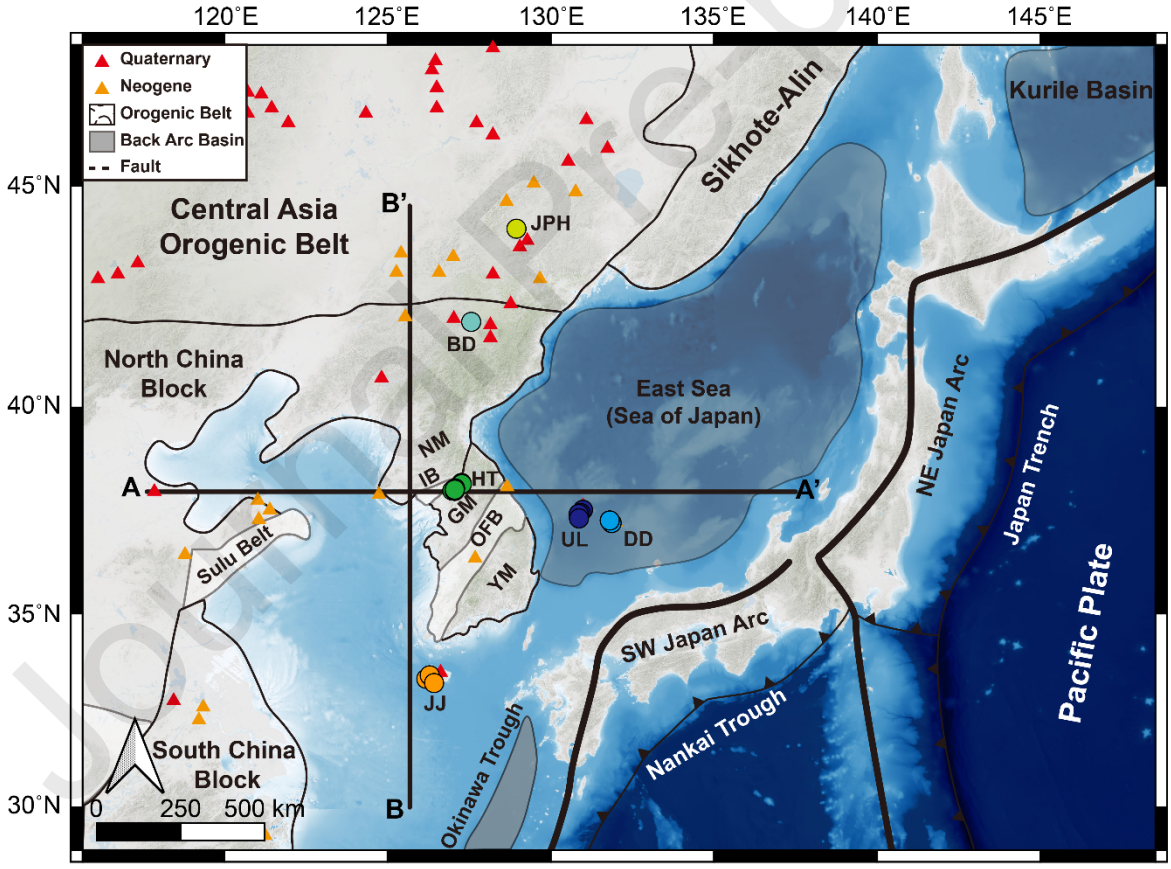

Fig. 1. Regional map of Northeast Asia showing locations of the basalt samples analyzed in this study. Abbreviations in the diagram are NM (Nangrim Massif), GM (Gyeonggi Massif), YM (Yeongnam Massif), IB (Imjingang Belt), OFB (Okcheon Fold Belt), JJ (Jeju Island), UL (Ulleung Island), DD (Dokdo Island), HT (Hantangang), BD (Baekdusan),

and JPH (Jingpohu), respectively. The solid lines of A-A' and B-B' represent cross-sections in the west-east and south-north directions, respectively (see Fig. 12).

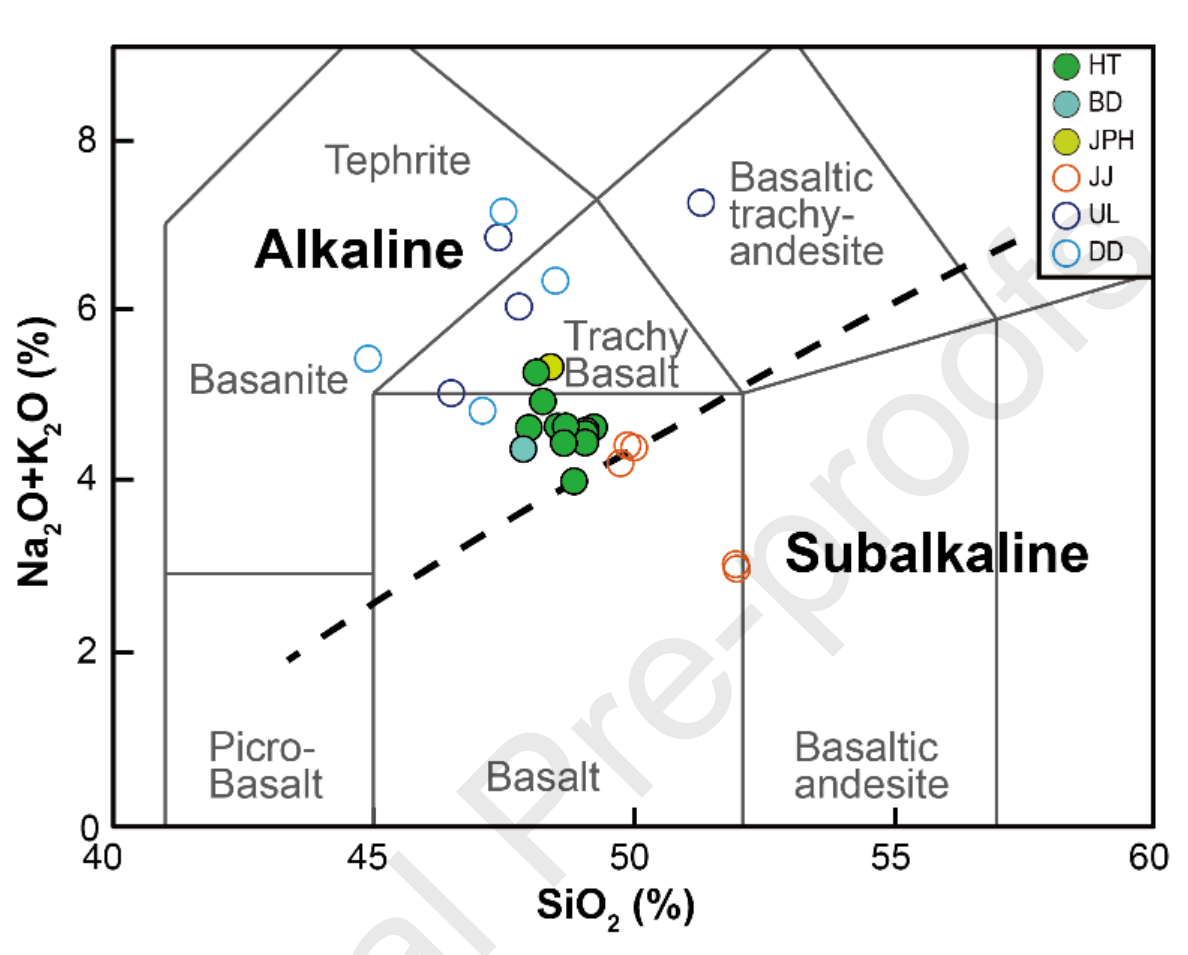

Fig. 2. Total alkali (Na_2O+K_2O) versus SiO_2 diagram (Le Bas et al., 1986) for the Korean Peninsula basalt samples.

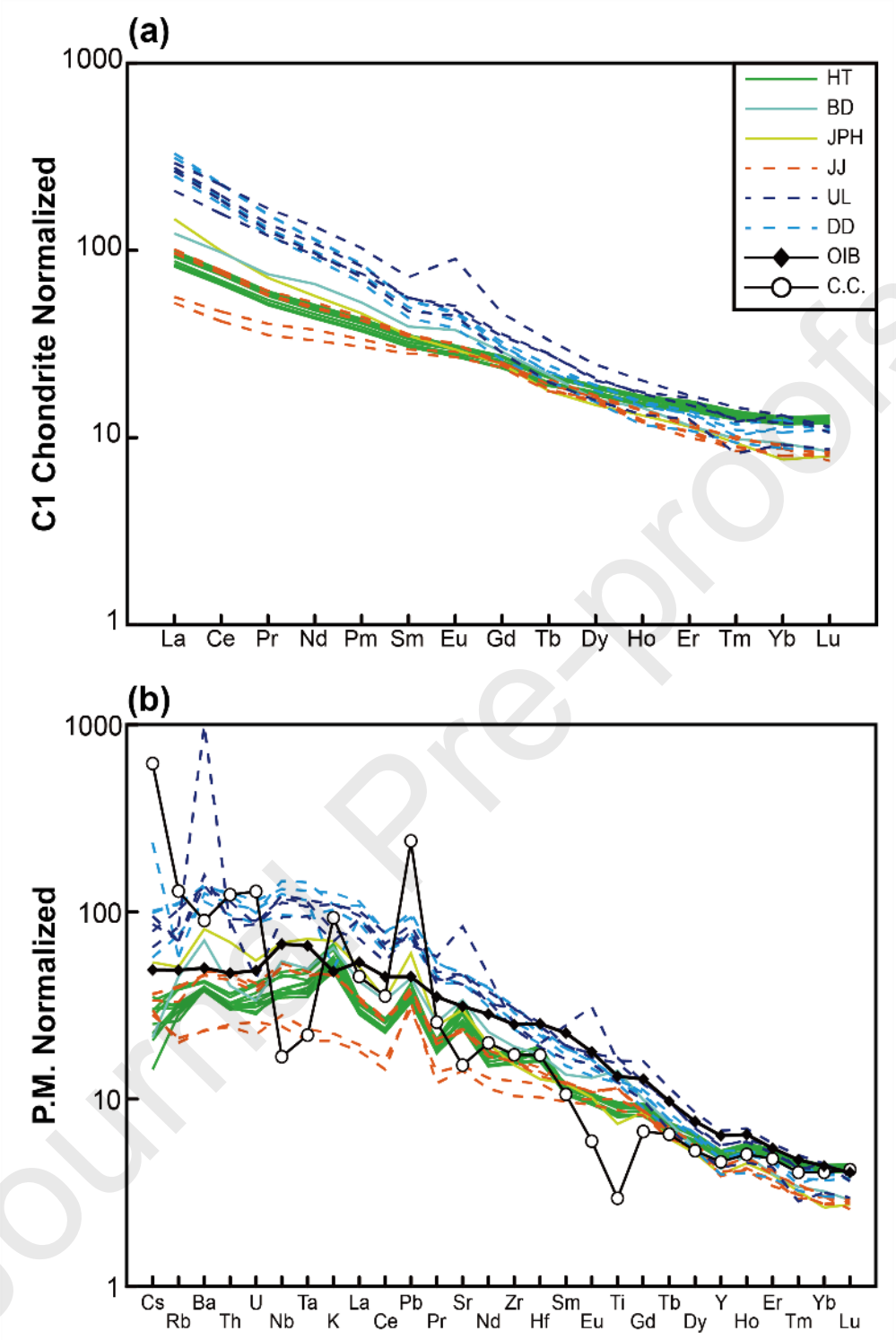

Fig. 3. (a) C1 chondrite-normalized rare earth element (REE) and (b) primitive mantle (PM) – normalized trace element patterns for the basalt samples (Sun and McDonough, 1989). Typical ocean island basalt (OIB) and upper continental crust compositions are from Sun and McDonough (1989) and Rudnick and Gao (2003).

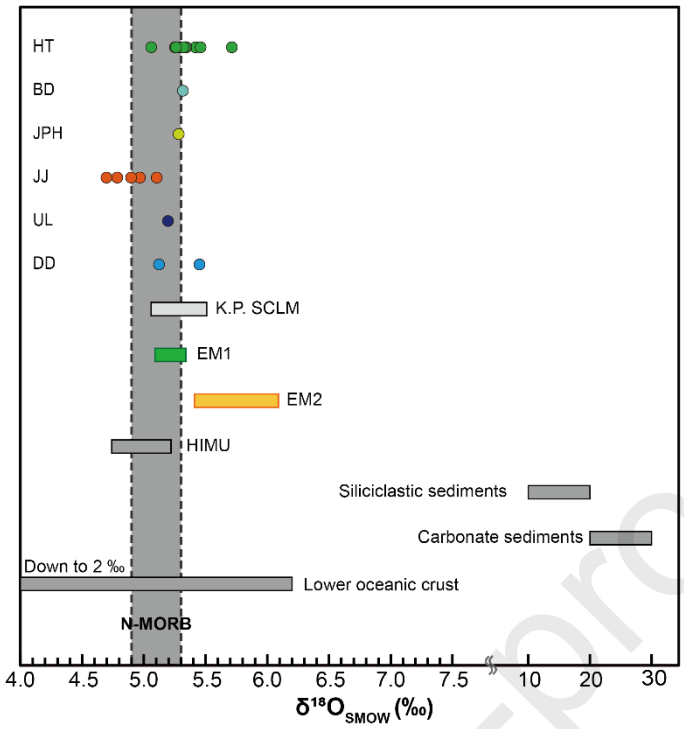

Fig. 4. Comprehensive comparison for $\delta^{18}O$ values of olivine phenocrysts in the basalt samples. The $\delta^{18}O$ range of the Korean Peninsula SCLM is from 5.1 to 5.5 ‰ (ultramafic xenoliths from Jeju-do, Jogok-ri, Baekryong-do, Baekdu-san, and Long Quan, Lee et al., 2013). The shaded vertical area represents $\delta^{18}O$ values of the N-MORB (4.9 to 5.3 ‰), and the $\delta^{18}O$ values of EM1, EM2, and HIMU are 5.1 to 5.3 ‰, 5.4 to 6.1 ‰, and 4.7 to 5.2 ‰, respectively (Eiler et al., 1997). The $\delta^{18}O$ range of the lower oceanic crust is 2.0 to 6.2 ‰, and the average $\delta^{18}O$ is 4.4 ‰ from gabbro in Site 735B (Hart et al., 1999). The $\delta^{18}O$ ranges of siliciclastic sediments and carbonate sediments are 10 to 20 ‰ and 20 to 30 ‰, respectively (Guo et al., 2013, and references therein).

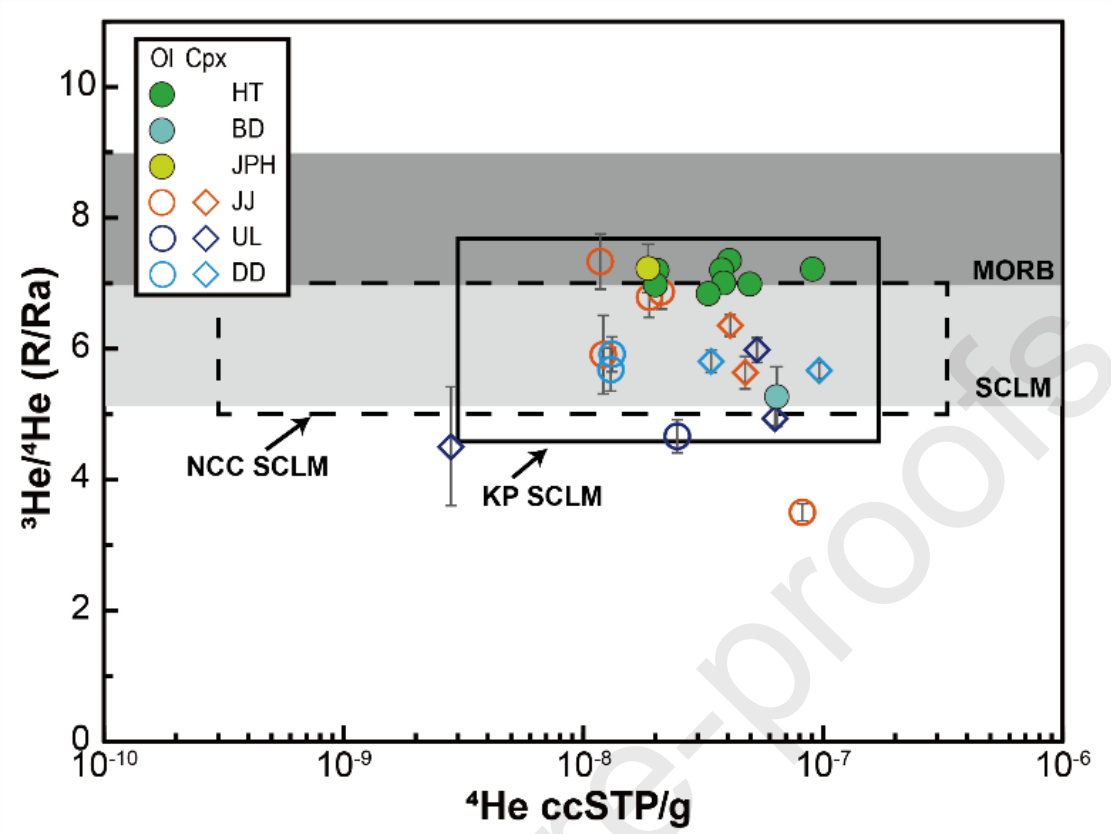

Fig. 5. Plot of ^{3}He/^{4}He ratios (R/R_a) versus ^{4}He contents of the basalt samples. Reference ^{3}He/^{4}He ratios are from Kim et al. (2021), Lee et al. (2021), and references therein. The ^{3}He/^{4}He ranges of the SCLM beneath the North China Block and the Korean Peninsula are from Chen et al. (2007) and Kim et al. (2005). The symbols are the same as in Fig. 2.

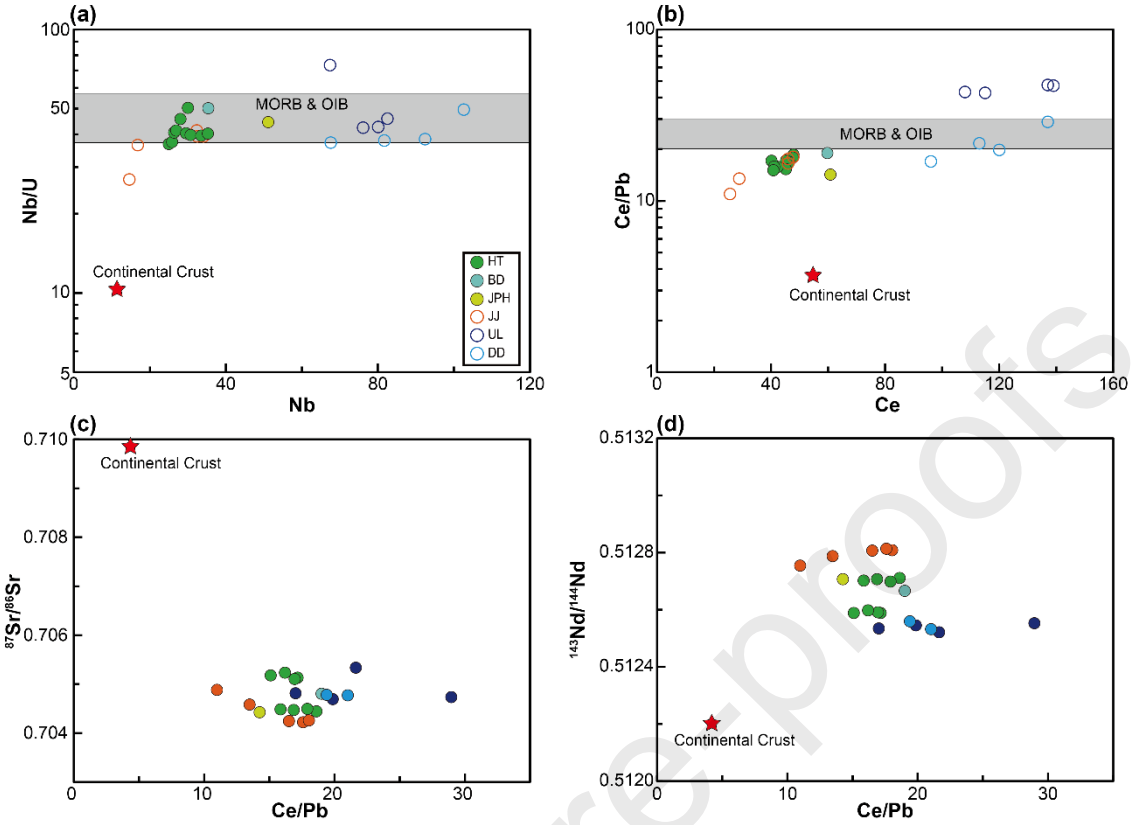

Fig. 6. Crustal assimilation indicators with (a) Nb/U vs. Nb (ppm). (b) Ce/Pb vs. Ce (ppm). (c) $^{87}Sr/^{86}Sr$ vs. Ce/Pb, (d) $^{143}Nd/^{144}Nd$ vs. Ce/Pb. The red star represents the upper continental crust (UCC) value (Rudnick and Gao, 2003). The shaded area means the OIB and MORB ranges (Nb/U: 37-57; Ce/Pb: 20-30; Hofmann et al., 1986).

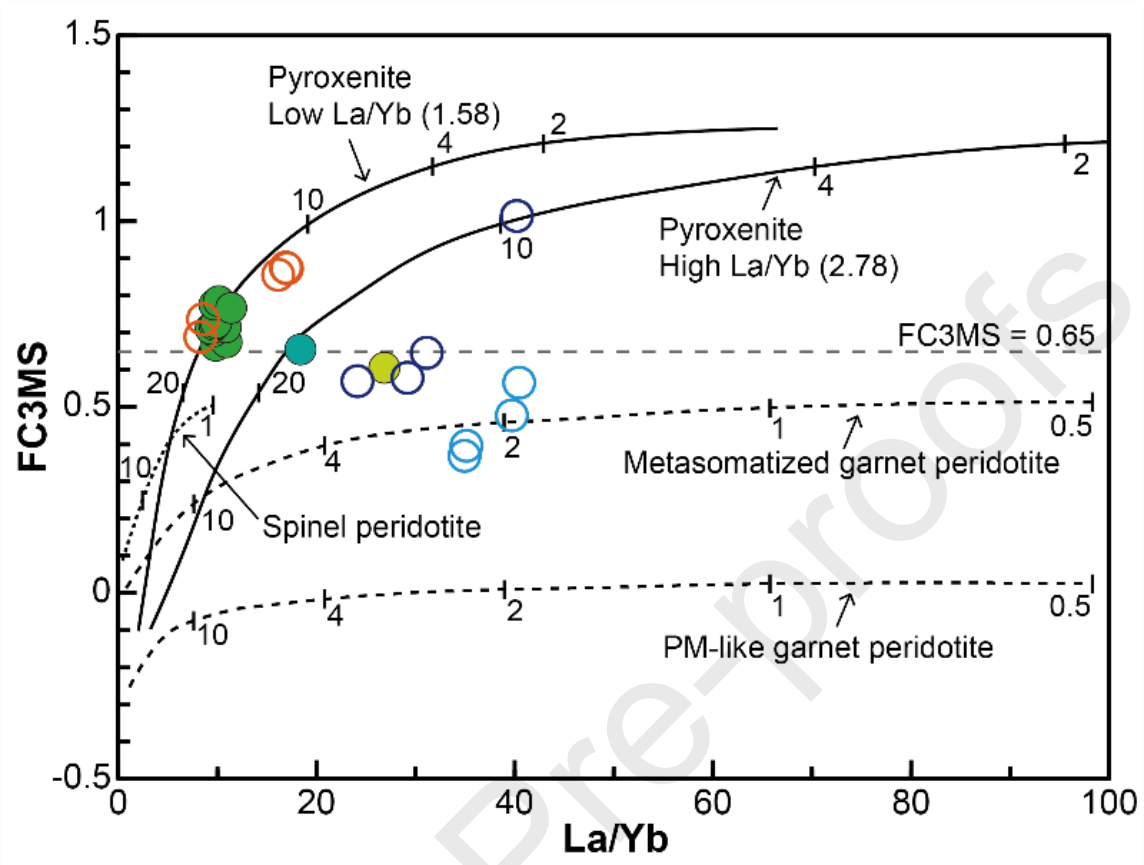

Fig. 7. La/Yb vs. FeO^T/CaO-3*MgO/SiO_2 (FC3MS) diagram after Yang et al. (2016). Numbers on curves denote the degree of partial melting. The two solid and three dashed curves are melting trends from pyroxenite with low (1.58) and high (2.78) La/Yb and garnet and spinel peridotites, and details of the melting models are described in Yang et al. (2016).

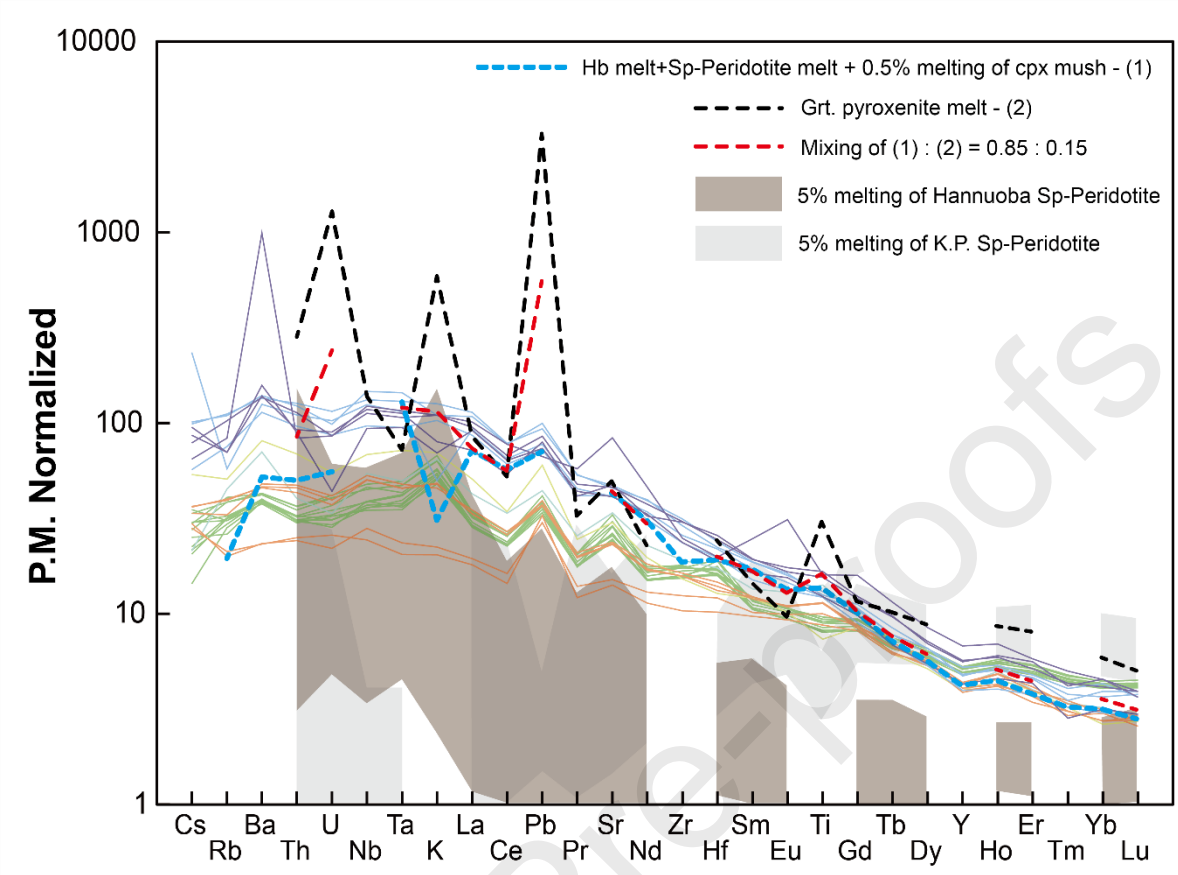

Fig. 8. P.M. normalized spider diagram (Sun and McDonough, 1989). (1) The blue dashed line is the ~35% partial melting of hornblendite + spinel-peridotite (Pilet et al., 2008) and the associated mixing with clinopyroxene mush-derived 0.5% partial melt by a ratio of 0.6:0.4 and modeled for Dokdo Island by Park et al. (2022). (2) The black dashed line is the averaged 5% partial melt of the garnet pyroxenite (Wang et al., 2016). The red dashed line is a mixture of partial melt (1) and garnet pyroxenite melt (2) by a ratio of 0.85:0.15. The grey and light grey shaded areas are 5% partial melting of non-modal batch melting of spinel peridotite mantle xenoliths from Hannuoba (Rudnick et al., 2004) and spinel peridotite mantle xenoliths from Korean Peninsula (Choi et al., 2005).

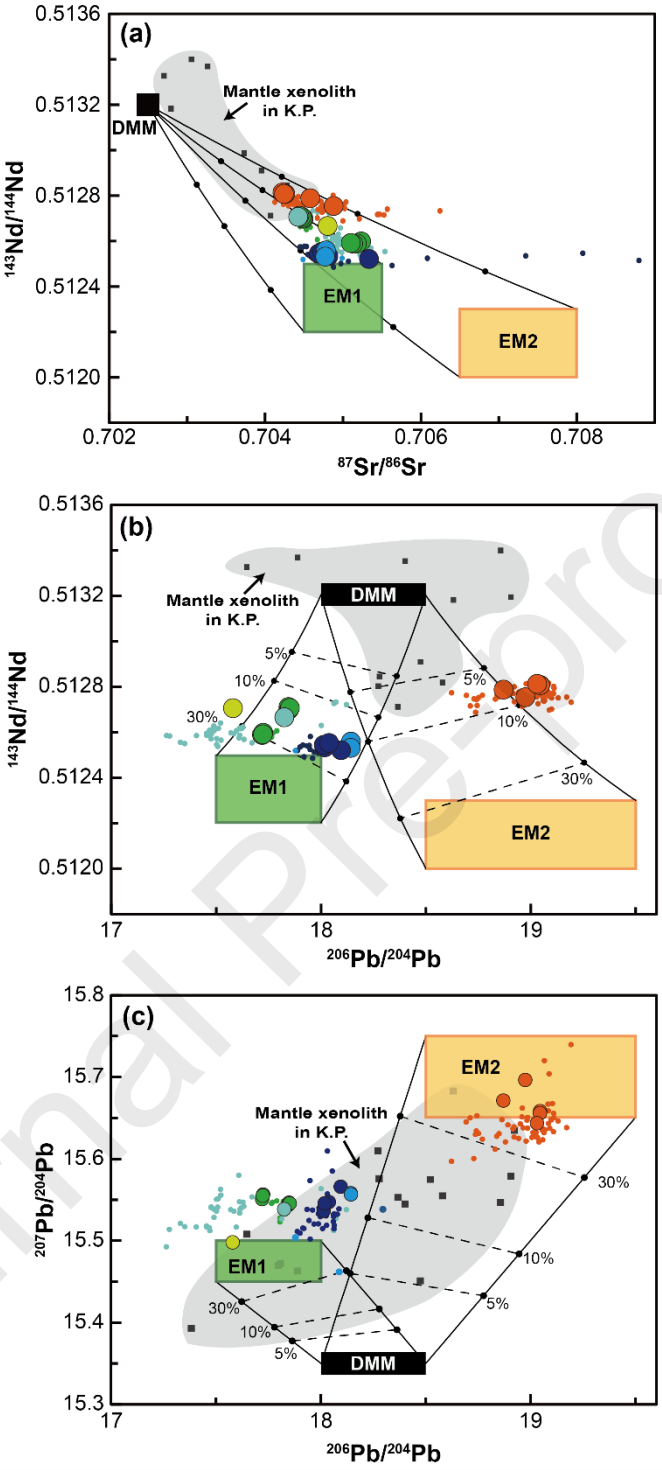

Fig. 9. Sr-Nd-Pb isotopic compositions of the samples and results of mixing calculation. Other small dots represent the isotopic compositions of other rocks from each volcanic field in previous studies (Choi et al., 2006; Choi et al., 2014; Choi et al., 2020; Choi, 2021; Kim et al., 2019a; Sakuyama et al., 2014). The grey area with a small grey square represents the isotopic composition of the K.P. SCLM (Choi et al., 2005). The black and dashed lines indicate mixing between EM1 and DMM, as well as between EM2 and DMM.

The composition of each end-member is in SCLM in Table S5.

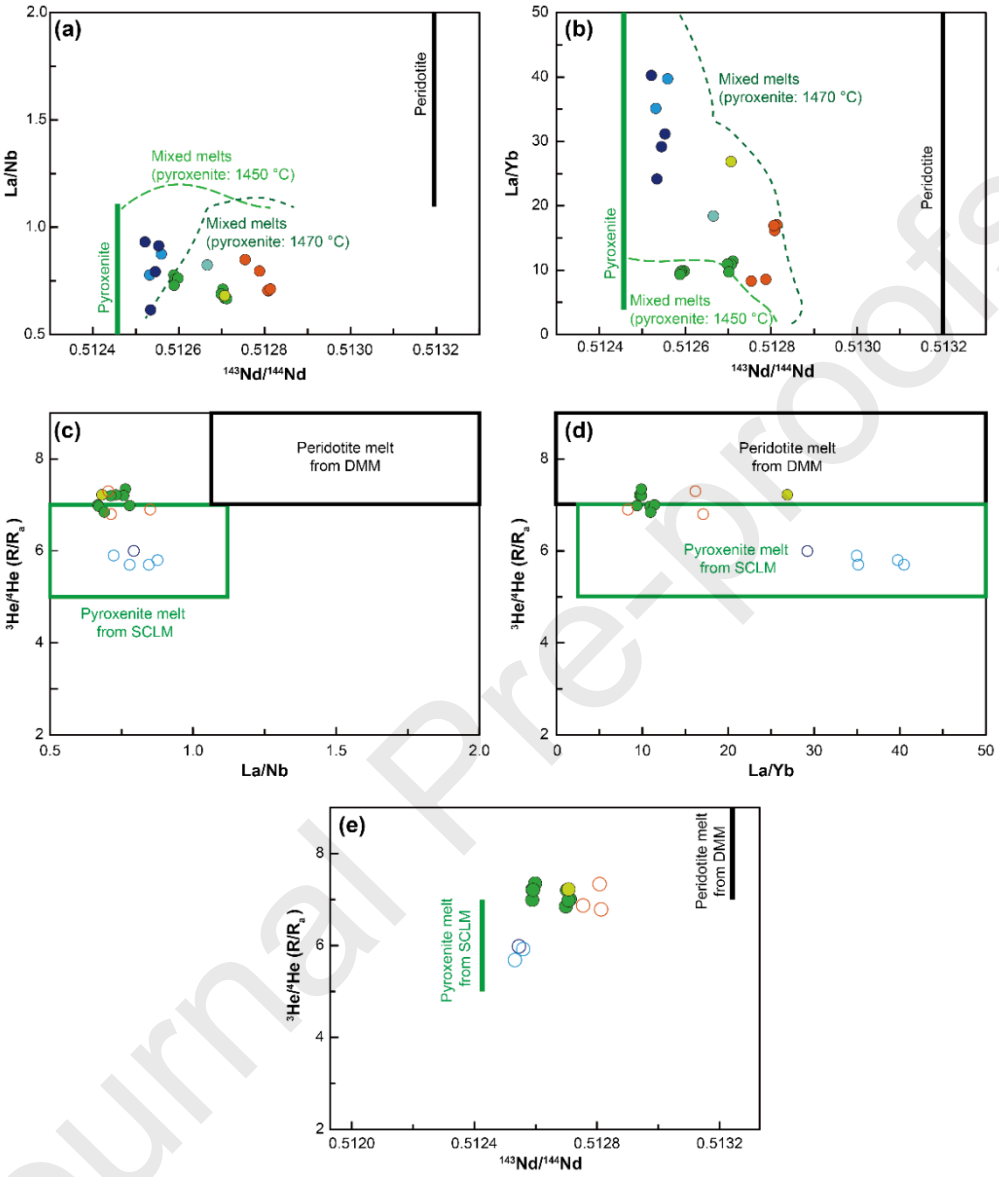

Fig. 10. (a) and (b) The composition of pyroxenite melt and peridotite melt were calculated by Stracke and Bourdon (2009). The pyroxenite represents a mixture of 85% 2 Ga old subduction-modified MORB and 15% lower continental crust, which is isotopically similar to EM-1. The peridotite composition is the average depleted mantle. The dashed green lines represent the mixture of melts from peridotite and pyroxenite (assuming peridotite: pyroxenite = 90: 10) with solidus temperatures (1450 °C and 1470 °C). (c), (d), and (e) illustrate the assumed compositions of pyroxenite and peridotite melts. It is assumed that the pyroxenite resides in the SCLM with low $^{3}He/^{4}He$ ratios (5 to 7 R_a), whereas the peridotite source is located in DMM with high $^{3}He/^{4}He$ ratios (7 to

9 R_a).

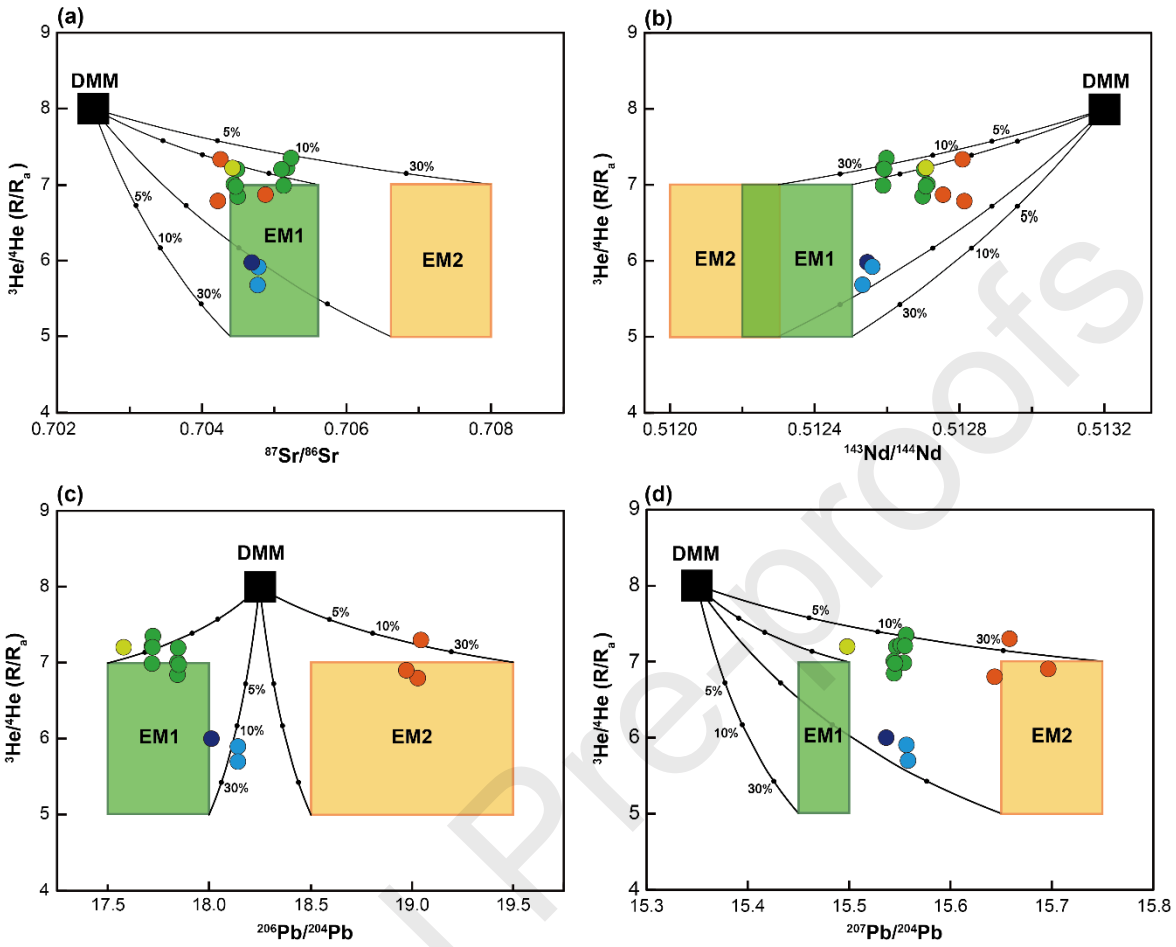

Fig. 11. The $^{3}He/^{4}He$ ratios with radiogenic isotopes and results of mixing calculations. Closed circles are considered to represent the helium isotopic ratios of the magma source samples. Open circles are samples that might not represent the magma source and could reflect plumbing system effects (degassing and differentiation) and secondary processes (diffusive fractionation). The lowest $^{3}He/^{4}He$ sample from JJ is a clear outlier and not in this figure. The composition of each end-member is assumed the EM1 and EM2 components in SCLM in Table S5.

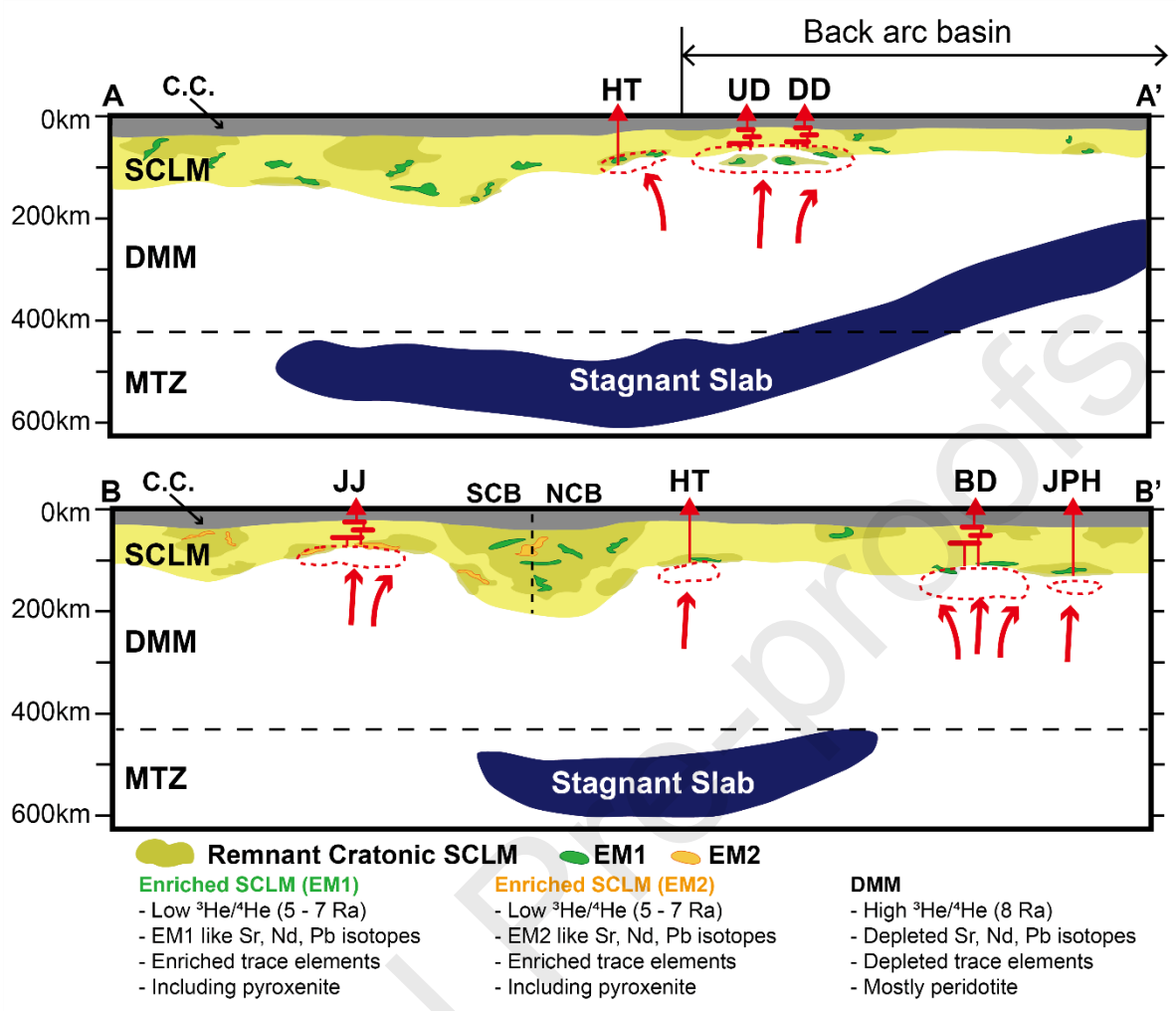

Fig. 12. Schematic illustration for magma generation of Cenozoic intraplate volcanism in Northeast Asia. The lithosphere and asthenosphere boundary and the location of the stagnant slab are considered 1300 K and 1600 K isotherms, respectively in mantle tomography from Lee et al. (2022). Abbreviations in the diagram are C.C. (continental crust), SCLM (subcontinental lithospheric mantle), DMM (depleted mid-ocean ridge basalt mantle), MTZ (matle transition zone), SCB (South China Block), and NCB (North China Block). The source magma produced by the upwelling of the hot asthenospheric mantle and its interaction with pyroxenite (EM1 and EM2) in the SCLM resulted in low $^{3}He/^{4}He$ ratios (5.7 to 7.3 Ra).

A-A': UD and DD are located in the back-arc basin, where the underlying SCLM experienced more severe deformation and potential delamination during the back-arc basin extension compared to other continental margins. The enriched SCLM beneath UD and DD caused more enriched trace element characteristics and lower $^{3}He/^{4}He$ ratios (6 Ra) compared to HT (7.3 Ra).

B-B': Mantle heterogeneity could generate differences in enriched materials within the SCLM. The enriched SCLM beneath JJ has EM2-like characteristics, while the enriched SCLM beneath HT, BD, and JPH exhibits EM1 signatures.

- We provide He-Sr-Nd-Pb-O isotopes of the Korean Peninsula basalts.
- The source lithology is a complex mixture of peridotite and pyroxenite sources.
- SCLM caused geochemical enrichment and low $^{3}He/^{4}He$ ratios in the basalts.

CRediT authorship contribution statement

D. Kim: Investigation, Writing – original draft, Writing – review & editing, Validation, Visualization, Methodology.

H. Lee: Conceptualization, Funding acquisition, Investigation, Project administration, Writing – original draft, Writing – review & editing, Validation, Visualization, Methodology.

M.J. Lee: Data curation, Investigation, Methodology, Validation, Visualization, Writing – original draft, Writing – review & editing.

C. Park: Data curation, Investigation, Methodology, Validation, Visualization, Writing – original draft, Writing – review & editing.

A.L. Rizzo: Data curation, Investigation, Methodology, Validation, Visualization, Writing – original draft, Writing – review & editing.

Declaration of competing interest

The authors declare that they have no known competing financial interests or personal relationships that could have appeared to influence the work reported in this paper.